# Image reconstruction in quantitative PAT with the simplified $P_2$ approximation

Christina Frederick\* Kui Ren $^{\dagger}$  Sarah Vallélian $^{\ddagger}$  May 12, 2018

#### Abstract

Photoacoustic tomography (PAT) is a hybrid imaging modality that intends to construct high-resolution images of optical properties of heterogeneous media from measured acoustic data generated by the photoacoustic effect. To date, most of the model-based quantitative image reconstructions in PAT are performed with either the radiative transport equation or its classical diffusion approximation as the model of light propagation. In this work, we study quantitative image reconstructions in PAT using the simplified  $P_2$  equations as the light propagation model. We provide numerical evidences on the feasibility of this approach and derive some stability results as theoretical justifications.

**Key words.** Photoacoustic tomography, radiative transport equation, simplified  $P_2$  approximation, diffusion approximation, hybrid inverse problems, hybrid imaging, image reconstruction, numerical optimization.

AMS subject classifications 2010. 35R30, 65M32, 65Z05, 74J25, 78A60, 78A70, 80A23.

#### 1 Introduction

Photoacoustic tomography (PAT) is a hybrid imaging method that couples ultrasound imaging and optical tomography via the photoacoustic effect, enabling high-resolution imaging of optical contrasts of heterogeneous media. In a typical way to induce the photoacoustic effect, a short pulse of near infra-red (NIR) light is sent into an optically heterogeneous medium, such as a piece of biological tissue, which we denote as  $\Omega \in \mathbb{R}^3$ . In the light propagation process, a portion of the photons are absorbed by the medium. The absorbed energy

<sup>\*</sup>Department of Mathematical Sciences, New Jersey Institute of Technology, University Heights, New Jersey 07102; christin@njit.edu

<sup>&</sup>lt;sup>†</sup>Department of Mathematics and Institute for Computational Engineering and Sciences, The University of Texas, Austin, TX 78712; ren@math.utexas.edu

<sup>&</sup>lt;sup>‡</sup>Department of Mathematics, North Carolina State University, Raleigh, NC 27695; scvallel@ncsu.edu

causes the medium to heat up slightly, and then cool down after the rest of the photons exit. The heating and cooling of the medium forces the medium to expand and then contract. This expansion and contraction generates a pressure field inside the medium which then propagates outwards in the form of ultrasound. The objective of PAT is to measure the ultrasound signals on the surface of the medium and use the measured data to recover information on the interior optical properties of the underlying medium. Interested readers are referred to [8, 14, 21, 43, 45, 50, 56, 67, 73, 74] for overviews of the physical principles as well as the practical applications of PAT.

The radiation of the photons inside the medium is described accurately by the phasespace radiative transport equation (RTE) [6, 7, 60]. Let us denote by  $u(\mathbf{x}, \mathbf{v})$  the density of photons at location  $\mathbf{x} \in \Omega$ , traveling in direction  $\mathbf{v} \in \mathbb{S}^2$  ( $\mathbb{S}^2$  being the unit sphere in  $\mathbb{R}^3$ ), integrated over the period of the pulse. Then  $u(\mathbf{x}, \mathbf{v})$  solves:

$$\mathbf{v} \cdot \nabla u(\mathbf{x}, \mathbf{v}) + \sigma_a(\mathbf{x})u(\mathbf{x}, \mathbf{v}) = \sigma_s(\mathbf{x})K(u)(\mathbf{x}, \mathbf{v}) \text{ in } X$$

$$u(\mathbf{x}, \mathbf{v}) = f(\mathbf{x}) \text{ on } \Gamma_-$$
(1)

Here  $X = \Omega \times \mathbb{S}^2$  is the phase space of photon propagation, with  $\Gamma_- = \{(\mathbf{x}, \mathbf{v}) : (\mathbf{x}, \mathbf{v}) \in \partial \Omega \times \mathbb{S}^2 \text{ s.t. } -\mathbf{n}(\mathbf{x}) \cdot \mathbf{v} > 0\}$  denoting the incoming boundary of X ( $\mathbf{n}(\mathbf{x})$  being the outer normal vector at  $\mathbf{x} \in \partial \Omega$ ). The positive functions  $\sigma_a(\mathbf{x})$  and  $\sigma_s(\mathbf{x})$  are respectively the absorption and the scattering coefficients of the medium. The function  $f(\mathbf{x})$  denotes the incoming illumination photon source, again integrated over the period of the pulse. To simplify the presentation, we have chosen the illumination source to be isotropic, i.e. independent of  $\mathbf{v}$ . This is by no means technically necessary.

The scattering operator K is defined as

$$K(u)(\mathbf{x}, \mathbf{v}) = \int_{\mathbb{S}^2} \Theta(\mathbf{v}, \mathbf{v}') u(\mathbf{x}, \mathbf{v}') d\mathbf{v}' - u(\mathbf{x}, \mathbf{v})$$

where the kernel  $\Theta(\mathbf{v}, \mathbf{v}')$  describes how photons traveling in direction  $\mathbf{v}'$  are scattered into direction  $\mathbf{v}$ , and also satisfies the normalization condition  $\int_{\mathbb{S}^2} \Theta(\mathbf{v}, \mathbf{v}') d\mathbf{v}' = \int_{\mathbb{S}^2} \Theta(\mathbf{v}', \mathbf{v}) d\mathbf{v}' = 1$ ,  $\forall \mathbf{v} \in \mathbb{S}^2$ . In practical applications in biomedical optics,  $\Theta$  is often taken to be the Henyey-Greenstein phase function, which depends only on the product  $\mathbf{v} \cdot \mathbf{v}'$ . That is,  $\Theta = \Theta_{HG}(\mathbf{v} \cdot \mathbf{v}')$  [6, 61]:

$$\Theta_{HG}(\mathbf{v}\cdot\mathbf{v}') = \frac{1}{4\pi} \frac{1-g^2}{(1+g^2-2g\mathbf{v}\cdot\mathbf{v}')^{3/2}},$$

where g is the scattering anisotropy factor of the medium.

The pressure field generated at a position  $\mathbf{x} \in \Omega$ , due to the photoacoustic effect, is the product of the Grüneisen coefficient, denoted by  $\Xi$ , and the absorbed energy density at  $\mathbf{x}$ . That is,

$$H = H^{rte}(\mathbf{x}) = \Xi(\mathbf{x})\sigma_a(\mathbf{x}) \int_{\mathbb{S}^2} u(\mathbf{x}, \mathbf{v}) d\mathbf{v}.$$
 (2)

The Grüneisen coefficient  $\Xi$  is a parameter that measures the local photoacoustic efficiency of the medium.

This initial pressure field then evolves following the acoustic wave equation in the form of ultrasound. The equation for the evolution reads [8, 14, 43, 50]:

$$\frac{1}{c^{2}(\mathbf{x})} \frac{\partial^{2} p}{\partial t^{2}} - \Delta p = 0, \text{ in } \mathbb{R}_{+} \times \Omega$$

$$p(t, \mathbf{x}) = H(\mathbf{x}), \quad \frac{\partial p}{\partial t}(t, \mathbf{x}) = 0, \text{ in } \{0\} \times \Omega$$

$$\mathbf{n} \cdot \nabla p(t, \mathbf{x}) = 0, \text{ on } \mathbb{R}_{+} \times \partial \Omega$$
(3)

where  $p(t, \mathbf{x})$  is the pressure field, and  $c(\mathbf{x})$  is the ultrasound wave speed. In the majority of the literature for PAT, the ultrasound speed is assumed known.

The data measured in PAT are the ultrasound signals on the surface of the medium for a long enough time period T, that is,  $p(t, \mathbf{x})_{|(0,T)\times\partial\Omega}$ . From the measured data, we attempt to infer information on the optical properties of the underlying medium, for instance, the coefficients  $\sigma_a$ ,  $\sigma_s$  and  $\Xi$ . This inverse problem has been extensively investigated in the past decade, from mathematical, computational as well as practical perspectives; see for instance [2, 3, 4, 5, 13, 15, 17, 18, 19, 20, 29, 35, 36, 37, 39, 44, 46, 49, 54, 55, 56, 58, ?, 65, 68, 69, 72, 76, 77, 78] and references therein.

In most of the past research in PAT, simplified mathematical models have been used as the model for light propagation, mainly due to the fact that the radiative transport model (1) is a phase-space model and is therefore computationally expensive to solve. The diffusion approximation to RTE, see (12), is the most commonly-used replacement model [12, 22]. While the diffusion approximation is much simpler for mathematical analysis and computational solution, it often suffers in terms of accuracy, especially in regions close to the source locations, a phenomenon that has been addressed extensively in the literature of optical tomography [6, 34, 71], as well as PAT [70]. In this work, we study the PAT inverse problem with the simplified  $P_2$  equations [1, 48], a more sophisticated approximation than the classical diffusion model to the radiative transport equation, as the model of light propagation. We show numerically that image reconstructions based on the simplified  $P_2$  model, while computationally less expensive than RTE-based reconstructions, can be more accurate than those based on the classical diffusion model under right circumstances.

We make the following general assumptions in the rest of the paper:

 $(\mathcal{A}\text{-i})$  the domain  $\Omega$  is simply-connected with smooth boundary  $\partial\Omega$ ;  $(\mathcal{A}\text{-ii})$  the physical coefficients  $(c, \Xi, \sigma_a, \sigma_s)$  are positive and bounded in the sense that  $0 < \underline{\alpha} \leq c, \Xi, \sigma_a, \sigma_s \leq \overline{\alpha} < \infty$  for some positive constants  $\underline{\alpha}$  and  $\overline{\alpha}$ ;  $(\mathcal{A}\text{-iii})$  the ultrasound speed function  $c(\mathbf{x})$  and the Grüneisen coefficient  $\Xi(\mathbf{x})$  are smooth in  $\Omega$ ; and  $(\mathcal{A}\text{-iv})$  the values of the coefficients are known on the boundary  $\partial\Omega$ .

The rest of the paper is structured as follows. We first review briefly in Section 2 the simplified  $P_2$  approximation to the radiative transport equation. We then present in Section 3 the main computational reconstruction algorithm we use for our numerical studies. In Section 4 we study the quantitative step of the inverse problems based on the simplified  $P_2$  equations. Detailed numerical simulation results based on synthetic data are presented in Section 5 to demonstrate the feasibility of our approach. Concluding remarks are offered in Section 6.

# 2 The simplified $P_2$ approximation

The radiative transport equation (1), although often regarded as an accurate mathematical model for light propagation in tissue-like optical media, is mathematically challenging to analyze and computationally expensive to solve. Macroscopic approximations to the RTE are often sought as alternative light propagation models.

A classic approach approximates the transport solution  $u(\mathbf{x}, \mathbf{v})$  using its first N moments in the direction variable  $\mathbf{v}$  [6, 27, 53]. This can be done, for example, via the spherical harmonics expansion. The  $P_N$  approximation is the system of derived equations for the coefficients of the expansion, i.e., the spherical harmonic moments. The standard diffusion approximation, i.e. the  $P_1$  approximation, to the RTE is obtained when only the zeroth moment is kept in the spherical harmonic expansion.

A major drawback of the classical  $P_N$  approximation is that the number of equations in the system grows as  $(N+1)^2$ , due to the rapid growth of the number of spherical harmonic modes as the order N increases. This problem is avoided in the simplified  $P_N$  approximation where the number of equations involved only grows linearly with respect to N. In the rest of this work, we will only focus on the simplified  $P_2$  equations. We refer interested readers to [31, 42, 48, 75] and the references therein for details on the derivation and numerical validation of the general simplified  $P_N$  ( $N \ge 1$ ) equations.

To introduce the simplified  $P_2$  approximation, we first define the following sequence of total absorption coefficients:

$$\sigma_{an}(\mathbf{x}) = \sigma_a(\mathbf{x}) + (1 - g^n)\sigma_s(\mathbf{x}), \qquad n \ge 0.$$
(4)

We also define the diffusion coefficients:

$$D(\mathbf{x}) = \frac{1}{3\sigma_{a1}(\mathbf{x})}, \quad \text{and} \quad \widetilde{D}(\mathbf{x}) = \frac{1}{7\sigma_{a3}(\mathbf{x})}.$$
 (5)

Then the simplified  $P_2$  equations, together with its boundary conditions, take the following form [42, 48, 75]:

$$-\nabla \cdot D\nabla \phi_{1}(\mathbf{x}) + \sigma_{a}\phi_{1}(\mathbf{x}) - \frac{2}{3}\sigma_{a}\phi_{2}(\mathbf{x}) = 0, \quad \text{in } \Omega$$

$$-\nabla \cdot \widetilde{D}\nabla \phi_{2}(\mathbf{x}) + (\frac{5}{9}\sigma_{a2} + \frac{4}{9}\sigma_{a})\phi_{2}(\mathbf{x}) - \frac{2}{3}\sigma_{a}\phi_{1}(\mathbf{x}) = 0, \quad \text{in } \Omega$$

$$\mathbf{n} \cdot D\nabla \phi_{1} + \frac{1}{2}\phi_{1} - \frac{1}{8}\phi_{2} = \frac{1}{2}f(\mathbf{x}), \quad \text{on } \partial\Omega$$

$$\mathbf{n} \cdot \widetilde{D}\nabla \phi_{2} + \frac{7}{24}\phi_{2} - \frac{1}{8}\phi_{1} = -\frac{1}{8}f(\mathbf{x}), \quad \text{on } \partial\Omega$$

$$(6)$$

where  $\phi_1$  and  $\phi_2$  are the first two composites, i.e. linear combinations of, Legendre moments of the transport solution  $u(\mathbf{x}, \mathbf{v})$ ; see [31, 42, 48, 75] for more details.

The initial pressure field generated due to the photoacoustic effect, corresponding to (2), can be written as follows in the simplified  $P_2$  approximation:

$$H = H^{P_2}(\mathbf{x}) = \Xi(\mathbf{x})\sigma_a(\mathbf{x})(\phi_1 - \frac{2}{3}\phi_2). \tag{7}$$

To simplify the analysis, we assume in the following that the absorption coefficient  $\sigma_a$  is very small compared to the effective scattering coefficient  $(1-g)\sigma_s$ , i.e.  $\sigma_a \ll (1-g)\sigma_s$ . Under

this assumption, we can neglect the factor  $\sigma_a$  in the definitions of the diffusion coefficients  $(D, \widetilde{D})$  and the absorption coefficients  $\sigma_{an}$  such that

$$\sigma_{a0} = \sigma_a, \qquad \sigma_{an} = (1 - g^n)\sigma_s, \quad n \ge 1, \qquad D(\mathbf{x}) = \frac{1}{3(1 - g)\sigma_s(\mathbf{x})},$$

$$\widetilde{D}(\mathbf{x}) = \frac{3}{7(1 + g + g^2)}D(\mathbf{x}), \qquad \sigma_{a2} = \frac{1 + g}{3}\frac{1}{D}.$$
(8)

We note that this assumption is not unfounded, as this is one of the assumptions under which (simplified)  $P_N$ -type approximations are shown to be valid. Moreover, in applications of PAT for biological tissues,  $\frac{\sigma_a}{(1-g)\sigma_s}$  is on the order of  $10^{-2} \ll 1$  [41].

With the simplification in (8), the simplified  $P_2$  system (6) reduces to the following form:

$$-\nabla \cdot D\nabla \phi_{1} + \sigma_{a}\phi_{1} - \frac{2}{3}\sigma_{a}\phi_{2} = 0, \quad \text{in } \Omega$$

$$-\nabla \cdot D\nabla \phi_{2} + (\frac{5}{9\kappa'}\frac{1}{D} + \frac{4}{9\kappa}\sigma_{a})\phi_{2} - \frac{2}{3\kappa}\sigma_{a}\phi_{1} = 0, \quad \text{in } \Omega$$

$$\mathbf{n} \cdot D\nabla \phi_{1} + \frac{1}{2}\phi_{1} - \frac{1}{8}\phi_{2} = \frac{1}{2}f(\mathbf{x}), \quad \text{on } \partial\Omega$$

$$\mathbf{n} \cdot D\nabla \phi_{2} + \frac{7}{24\kappa}\phi_{2} - \frac{1}{8\kappa}\phi_{1} = -\frac{1}{8\kappa}f(\mathbf{x}), \quad \text{on } \partial\Omega$$
(9)

where

$$\kappa = \frac{3}{7(1+q+q^2)}, \quad \text{and} \quad \kappa' = \frac{3}{1+q}\kappa.$$

The corresponding initial pressure field  $H^{P_2}$  in (7) remains in the same form.

It is sometimes more convenient to rewrite the simplified  $P_2$  system (9) in a new pair of variables  $(\varphi_1, \varphi_2)$ :  $\varphi_1 = \phi_1 - \frac{2}{3}\phi_2$  and  $\varphi_2 = \phi_2$ . In this case, we have

$$-\nabla \cdot D\nabla \varphi_{1} + (1 + \frac{4}{9\kappa})\sigma_{a}\varphi_{1} - \frac{10}{27\kappa'}\frac{1}{D}\varphi_{2} = 0, \quad \text{in } \Omega$$

$$-\nabla \cdot D\nabla \varphi_{2} + \frac{5}{9\kappa'}\frac{1}{D}\varphi_{2} - \frac{2}{3\kappa}\sigma_{a}\varphi_{1} = 0, \quad \text{in } \Omega$$

$$\mathbf{n} \cdot D\nabla \varphi_{1} + \frac{6\kappa+1}{12\kappa}\varphi_{1} + \frac{15\kappa-10}{72\kappa}\varphi_{2} = \frac{6\kappa+1}{12\kappa}f(\mathbf{x}), \quad \text{on } \partial\Omega$$

$$\mathbf{n} \cdot D\nabla \varphi_{2} + \frac{5}{24\kappa}\varphi_{2} - \frac{1}{8\kappa}\varphi_{1} = -\frac{1}{8\kappa}f(\mathbf{x}), \quad \text{on } \partial\Omega$$

$$(10)$$

The corresponding initial pressure field can now be written as

$$H = H^{P_2'}(\mathbf{x}) = \Xi(\mathbf{x})\sigma_a(\mathbf{x})\varphi_1(\mathbf{x}). \tag{11}$$

To recover the classical diffusion approximation to the radiative transport equation, we drop the terms involve gradient of  $u_2$  from the simplified  $P_2$  system (10). This leads to the simplified  $P_1$  approximation:

$$-\nabla \cdot D(\mathbf{x})\nabla \varphi(\mathbf{x}) + \sigma_a(\mathbf{x})\varphi(\mathbf{x}) = 0, \quad \text{in } \Omega$$
$$\mathbf{n} \cdot D\nabla \varphi + \frac{1}{2}\varphi = \frac{1}{2}f(\mathbf{x}), \quad \text{on } \partial\Omega$$
 (12)

The corresponding initial pressure field generated in this case takes the form:

$$H = H^{diff}(\mathbf{x}) = \Xi(\mathbf{x})\sigma_a(\mathbf{x})\varphi(\mathbf{x}). \tag{13}$$

Note that  $\varphi_1$  in (10) and  $\varphi$  in (12) are different approximations to the same physical quantity, the photon density. We use different symbols here for the two to avoid unnecessary confusion.

Moreover, the boundary condition in the diffusion approximation (12), i.e. simplified  $P_1$  approximation, is slightly different from the boundary condition one can obtain from a detailed boundary layer analysis in the classical  $P_1$  approximations [23]. For the sake of consistency, we use the boundary condition in (12).

It is well-known that under reasonable regularity assumptions on the optical coefficients  $(\sigma_a, \sigma_s)$  and the boundary illumination source f, the radiative transport equation (1) and its diffusion approximation (12) are well-posed in appropriate function spaces [23]. Therefore the initial pressure fields  $H^{rte}$  and  $H^{diff}$  are well-defined quantities. The simplified  $P_2$  system is less studied. It is straightforward to verify from standard theory of elliptic systems [32, 52] that the simplified  $P_2$  system (9) is also well-posed under similar assumptions. Therefore,  $H^{P_2}$  is also a well-defined quantity.

# 3 Numerical reconstruction algorithms

In this section, we implement a standard optimal control-based numerical image reconstruction algorithm for PAT with the simplified  $P_2$  equations (9) and the classical diffusion equation (12) as the models of light propagation. Due to the fact that the data we have is not enough to uniquely determine all three coefficients  $(\Xi, \sigma_a, \sigma_s)$  simultaneously [10, 51], we consider here only the reconstruction of two coefficients. We provide the details for the case of reconstructing  $(\sigma_a, \sigma_s)$ . Reconstructing other pairs, such as  $(\Xi, \sigma_a)$ , can be done very similarly.

Let us assume that we have data collected from  $J \geq 2$  different illuminations  $\{f_j\}_{j=1}^J$ . We denote by  $\{p_j^*\}_{j=1}^J$  the measured ultrasound data. We solve the reconstruction problem by searching for the coefficient pair  $(\sigma_a, \sigma_s)$  that minimize the mismatch between ultrasound data predicted by the mathematical models and the measurements. More precisely, we solve the minimization problem

$$\min_{\sigma_a, \sigma_s} \mathcal{O}(\sigma_a, \sigma_s), \text{ subject to, } \mathfrak{l}_a \le \sigma_a \le \mathfrak{u}_a, \mathfrak{l}_s \le \sigma_s \le \mathfrak{u}_s$$
 (14)

where the linear bounds  $\{\mathfrak{l}_a,\mathfrak{u}_a,\mathfrak{l}_s,\mathfrak{u}_s\}$  are selected in a case by case manner, as discussed further in the numerical simulations in Section 5. The data mismatch functional is defined as

$$\mathcal{O}(\sigma_a, \sigma_s) = \frac{1}{2} \sum_{j=1}^{J} \int_0^T \int_{\partial \Omega} (p_j^{\mathcal{M}} - p_j^*)^2 dS(\mathbf{x}) dt + \alpha \mathcal{R}(\sigma_a) + \beta \mathcal{R}(\sigma_s), \tag{15}$$

where  $p_j^{\mathcal{M}}$  is the ultrasound signal predicted using the light propagation model  $\mathcal{M} \in \{P_2, \text{diff}\}$  with the coefficient  $(\sigma_a, \sigma_s)$ . The parameters  $\alpha$  and  $\beta$  are used to control the strengths of the regularization mechanism encoded in the functional  $\mathcal{R}$ . The regularization functional we select here is of Tikhonov type, based on the  $L^2$  norm of the gradients,

$$\mathcal{R}(\sigma_a) = \frac{1}{2} \|\nabla \sigma_a\|_{(L^2(\Omega))^3}^2 \equiv \frac{1}{2} \int_{\Omega} |\nabla \sigma_a|^2 d\mathbf{x}.$$
 (16)

While we choose the same regularization functional for both  $\sigma_a$  and  $\sigma_s$  for convenience, it is not required. Other types of regularization can also be considered, but will not be discussed in this paper.

To solve the minimization problem (14), we use the SNOPT algorithm developed in [33]. In a nutshell, this is a sparse sequential quadratic programming (SQP) algorithm where the Hessian of the Lagrangian is approximated by a limited-memory BFGS strategy. This is a mature optimization technique, therefore we will not describe it in detail here. Our main objective is to supply the optimization algorithm with a subroutine to evaluate the mismatch functional  $\mathcal{O}$  and its derivatives with respect to the optical properties  $\sigma_a$  and  $\sigma_s$ . The derivatives can be computed in a standard manner using the adjoint state method. We summarize the calculations of the derivatives in the following lemma.

**Lemma 3.1.** Let  $\Omega$ , c and  $\Xi$  satisfy the assumptions in (A-i)-(A-iv) and assume that the assumptions in (8) hold as well. For each  $1 \leq j \leq J$ , let  $f_j(\mathbf{x})$  be the restriction of a  $C^1$  function to  $\partial\Omega$ . Then the predicted ultrasound data for illumination source  $f_j$  using specified optical model  $\mathcal{M}$ ,  $p_{j-|(0,T]\times\partial\Omega}^{\mathcal{M}}$ , viewed as the map:

$$p_{j}^{\mathcal{M}}|_{(0,T]\times\partial\Omega}: \begin{array}{ccc} (\sigma_{a},\sigma_{s}) & \mapsto & p_{j}^{\mathcal{M}}|_{(0,T]\times\partial\Omega} \\ \mathcal{C}^{1}(\bar{\Omega})\times\mathcal{C}^{1}(\bar{\Omega}) & \mapsto & \mathcal{H}^{1/2}((0,T]\times\partial\Omega) \end{array}$$
(17)

is Fréchet differentiable at any  $(\sigma_a, \sigma_s) \in C^1(\overline{\Omega}) \times C^1(\overline{\Omega})$  that satisfies the assumptions in (A-ii). Moreover, the mismatch functional  $\mathcal{O}(\sigma_a, \sigma_s) : C^1(\overline{\Omega}) \times C^1(\overline{\Omega}) \mapsto \mathbb{R}_+$  given by (15) is Fréchet differentiable and its derivatives at  $(\sigma_a, \sigma_s)$  in the directions  $\delta \sigma_a \in C_0^1(\overline{\Omega})$  and  $\delta \sigma_s \in C_0^1(\Omega)$  (such that  $\sigma_a + \delta \sigma_a$  and  $\sigma_s + \delta \sigma_s$  satisfy (A-ii)) are given as follows. Let  $q_j(t, \mathbf{x}), 1 \leq j \leq J$ , be the solution to the adjoint wave equation:

$$\frac{1}{c^{2}(\mathbf{x})} \frac{\partial^{2} q_{j}}{\partial t^{2}} - \Delta q_{j} = 0, \quad in (0, T) \times \Omega$$

$$q_{j}(t, \mathbf{x}) = 0, \quad \frac{\partial q_{j}}{\partial t}(t, \mathbf{x}) = 0, \quad in \{T\} \times \Omega$$

$$\mathbf{n} \cdot \nabla q_{j}(t, \mathbf{x}) = p_{j}^{\mathcal{M}} - p_{j}^{*}, \quad on (0, T) \times \partial\Omega$$
(18)

(i) If the optical model  $\mathcal{M}$  is the simplified  $P_2$  model (9), then

$$\mathcal{O}'(\sigma_{a}, \sigma_{s})[\delta\sigma_{a}] = \sum_{j=1}^{J} \int_{\Omega} (\phi_{1,j} - \frac{2}{3}\phi_{2,j}) \left\{ \frac{\Xi}{c^{2}} \frac{\partial q_{j}}{\partial t}(0, \mathbf{x}) + (\psi_{1,j} - \frac{2}{3\kappa}\psi_{2,j}) \right\} \delta\sigma_{a}(\mathbf{x}) d\mathbf{x}$$

$$+\alpha \mathcal{R}'(\sigma_{a})[\delta\sigma_{a}], \qquad (19)$$

$$\mathcal{O}'(\sigma_{a}, \sigma_{s})[\delta\sigma_{s}] = \sum_{j=1}^{J} \int_{\Omega} \left\{ \frac{\nabla \psi_{1,j} \cdot \nabla \psi_{1,j} + \nabla \phi_{2,j} \cdot \nabla \psi_{2,j}}{3(1-g)\sigma_{s}^{2}} - \frac{5(1-g^{2})}{9\kappa}\phi_{2,j}\psi_{2,j} \right\} \delta\sigma_{s}(\mathbf{x}) d\mathbf{x}$$

$$+\beta \mathcal{R}'(\sigma_{s})[\delta\sigma_{s}], \qquad (20)$$

where  $(\phi_{1,j},\phi_{2,j})$  solves (9) with source  $f_j$ ,  $1 \leq j \leq J$ , while  $(\psi_{1,j},\psi_{2,j})$  solves the adjoint

diffusion system:

$$-\nabla \cdot D\nabla \psi_{1,j} + \sigma_a(\psi_{1,j} - \frac{2}{3\kappa}\psi_{2,j}) = -\frac{\Xi}{c^2}\sigma_a\partial_t q_j(0, \mathbf{x}), \quad in \ \Omega$$

$$-\nabla \cdot D\nabla \psi_{2,j} + (\frac{5}{9\kappa'}\frac{1}{D} + \frac{4}{9\kappa}\sigma_a)\psi_{2,j} - \frac{2}{3}\sigma_a\psi_{1,j} = \frac{2}{3}\frac{\Xi}{c^2}\sigma_a\partial_t q_j(0, \mathbf{x}), \quad in \ \Omega$$

$$\mathbf{n} \cdot D\nabla \psi_{1,j} + \frac{1}{2}\psi_{1,j} - \frac{1}{8\kappa}\psi_{2,j} = 0, \quad on \ \partial\Omega$$

$$\mathbf{n} \cdot D\nabla \psi_{2,j} + \frac{7}{24\kappa}\psi_{2,j} - \frac{1}{8}\psi_{1,j} = 0, \quad on \ \partial\Omega$$

$$(21)$$

(ii) If the optical model  $\mathcal{M}$  is the classical diffusion model (12), then

$$\mathcal{O}'(\sigma_a, \sigma_s)[\delta \sigma_a] = \sum_{j=1}^{J} \int_{\Omega} \varphi_j \left\{ \frac{\Xi}{c^2} \frac{\partial q_j}{\partial t} (0, \mathbf{x}) + \eta_j \right\} \delta \sigma_a(\mathbf{x}) d\mathbf{x} + \alpha \mathcal{R}'(\sigma_a)[\delta \sigma_a],$$
(22)

$$\mathcal{O}'(\sigma_a, \sigma_s)[\delta \sigma_s] = \sum_{j=1}^{J} \int_{\Omega} \frac{\nabla \varphi_j \cdot \nabla \eta_j}{3(1-g)\sigma_s^2} \delta \sigma_s(\mathbf{x}) d\mathbf{x} + \beta \mathcal{R}'(\sigma_s)[\delta \sigma_s], \tag{23}$$

where  $\varphi_j$  solves (12) with source  $f_j$ ,  $1 \leq j \leq J$ , and  $\eta_j$  solves

$$-\nabla \cdot D(\mathbf{x})\nabla \eta_{j}(\mathbf{x}) + \sigma_{a}(\mathbf{x})\eta_{j}(\mathbf{x}) = -\frac{\Xi}{c^{2}}\sigma_{a}\partial_{t}q_{j}(0,\mathbf{x}), \quad in \ \Omega$$

$$\mathbf{n} \cdot D\nabla \eta_{j} + \frac{1}{2}\eta_{j} = 0, \quad on \ \partial\Omega$$
(24)

Proof. The result on the classical diffusion model (12) is proved in [25]. We focus here on the simplified  $P_2$  model. Under the assumptions stated in the lemma, standard elliptic theory in [32, 52] implies that (9) admits a unique solution pair  $(\phi_{1,j}, \phi_{2,j}) \in \mathcal{H}^2(\Omega) \times \mathcal{H}^2(\Omega)$  for source  $f_j$ . This, together with the assumption on  $\sigma_a$ , gives that the initial pressure field  $H_j^{\mathcal{M}} \in \mathcal{H}^1(\Omega)$ , which then ensures that the wave equation (3) admits a unique solution  $p_j^{\mathcal{M}} \in \mathcal{H}^1((0,T] \times \Omega)$  [24, 40, 59]. Differentiability of  $p_{j-|(0,T] \times \partial\Omega}^{\mathcal{M}}$  with respect to the initial pressure field  $H_j^{\mathcal{M}}$  then follows from the linearity of the map:  $\mathcal{H}^1(\Omega) \to \mathcal{H}^{1/2}((0,T] \times \partial\Omega)$  [24, 40]. It remains, following the chain rule, to show that  $H_j^{\mathcal{M}} : \mathcal{C}^1(\bar{\Omega}) \times \mathcal{C}^1(\bar{\Omega}) \mapsto \mathcal{H}^1(\Omega)$  is Fréchet differentiable with respect to  $\sigma_a$  and  $\sigma_s$ . We now prove this for the derivative with respect to  $\sigma_a$ . The other derivative follows from similar calculations.

Let  $(\phi_{1,j}^{(\sigma_a+\delta\sigma_a,\sigma_s)},\phi_{2,j}^{(\sigma_a+\delta\sigma_a,\sigma_s)})$  and  $(\phi_{1,j}^{(\sigma_a,\sigma_s)},\phi_{2,j}^{(\sigma_a,\sigma_s)})$  be the solution to the simplified  $P_2$  model (9) with coefficients  $(\sigma_a+\delta\sigma_a,\sigma_s)$  and  $(\sigma_a,\sigma_s)$  respectively, for source  $f_j$ . Let  $(\widetilde{\phi}_{1,j},\widetilde{\phi}_{2,j})$  be the solution to, with the notation  $\Delta\phi=\phi_{1,j}^{(\sigma_a,\sigma_s)}-\frac{2}{3}\phi_{2,j}^{(\sigma_a,\sigma_s)}$ ,

$$-\nabla \cdot D\nabla \widetilde{\phi}_{1,j} + \sigma_a(\widetilde{\phi}_{1,j} - \frac{2}{3}\widetilde{\phi}_{2,j}) = -\Delta \phi \delta \sigma_a, \text{ in } \Omega$$

$$-\nabla \cdot D\nabla \widetilde{\phi}_{2,j} + \frac{5}{9\kappa'} \frac{1}{D}\widetilde{\phi}_{2,j} - \frac{2\sigma_a}{3\kappa} (\widetilde{\phi}_{1,j} - \frac{2}{3}\widetilde{\phi}_{2,j}) = \frac{2}{3\kappa} \Delta \phi \delta \sigma_a, \text{ in } \Omega$$

$$\mathbf{n} \cdot D\nabla \widetilde{\phi}_{1,j} + \frac{1}{2}\widetilde{\phi}_{1,j} - \frac{1}{8}\widetilde{\phi}_{2,j} = 0, \text{ on } \partial\Omega$$

$$\mathbf{n} \cdot D\nabla \widetilde{\phi}_{2,j} + \frac{7}{24\kappa} \widetilde{\phi}_{2,j} - \frac{1}{8\kappa} \widetilde{\phi}_{1,j} = 0, \text{ on } \partial\Omega$$

$$(25)$$

We define  $\widehat{\phi}_{i,j} = \phi_{i,j}^{(\sigma_a + \delta \sigma_a, \sigma_s)} - \phi_{i,j}^{(\sigma_a, \sigma_s)}$  and  $\overline{\overline{\phi}}_{i,j} = \widehat{\phi}_{i,j} - \widetilde{\phi}_{i,j}$ , i = 1, 2. It is straightforward to check that  $(\widehat{\phi}_{1,j}, \widehat{\phi}_{2,j})$  solves

$$-\nabla \cdot D\nabla \widehat{\phi}_{1,j} + (\sigma_a + \delta\sigma_a)(\widehat{\phi}_{1,j} - \frac{2}{3}\widehat{\phi}_{2,j}) = -\Delta\phi\delta\sigma_a, \text{ in } \Omega$$

$$-\nabla \cdot D\nabla \widehat{\phi}_{2,j} + \frac{5}{9\kappa'} \frac{1}{D}\widehat{\phi}_{2,j} - \frac{2(\sigma_a + \delta\sigma_a)}{3\kappa}(\widehat{\phi}_{1,j} - \frac{2}{3}\widehat{\phi}_{2,j}) = \frac{2}{3\kappa}\Delta\phi\delta\sigma_a, \text{ in } \Omega$$

$$\mathbf{n} \cdot D\nabla \widehat{\phi}_{1,j} + \frac{1}{2}\widehat{\phi}_{1,j} - \frac{1}{8}\widehat{\phi}_{2,j} = 0, \text{ on } \partial\Omega$$

$$\mathbf{n} \cdot D\nabla \widehat{\phi}_{2,j} + \frac{7}{24\kappa}\widehat{\phi}_{2,j} - \frac{1}{8\kappa}\widehat{\phi}_{1,j} = 0, \text{ on } \partial\Omega$$

$$(26)$$

and  $(\overline{\overline{\phi}}_{1,j}, \overline{\overline{\phi}}_{2,j})$  solves

$$-\nabla \cdot D \nabla \overline{\overline{\phi}}_{1,j} + \sigma_{a} (\overline{\overline{\phi}}_{1,j} - \frac{2}{3} \overline{\overline{\phi}}_{2,j}) = -(\widehat{\phi}_{1,j} - \frac{2}{3} \widehat{\phi}_{2,j}) \delta \sigma_{a}, \text{ in } \Omega$$

$$-\nabla \cdot D \nabla \overline{\overline{\phi}}_{2,j} + \frac{5}{9\kappa'} \frac{1}{D} \overline{\overline{\phi}}_{2,j} - \frac{2}{3\kappa} \sigma_{a} (\overline{\overline{\phi}}_{1,j} - \frac{2}{3} \overline{\overline{\phi}}_{2,j}) = \frac{2}{3\kappa} (\widehat{\phi}_{1,j} - \frac{2}{3} \widehat{\phi}_{2,j}) \delta \sigma_{a}, \text{ in } \Omega$$

$$\mathbf{n} \cdot D \nabla \overline{\overline{\phi}}_{1,j} + \frac{1}{2} \overline{\overline{\phi}}_{1,j} - \frac{1}{8} \overline{\overline{\phi}}_{2,j} = 0, \text{ on } \partial \Omega$$

$$\mathbf{n} \cdot D \nabla \overline{\overline{\phi}}_{2,j} + \frac{7}{24\kappa} \overline{\overline{\phi}}_{2,j} - \frac{1}{8\kappa} \overline{\overline{\phi}}_{1,j} = 0, \text{ on } \partial \Omega$$

Note that in the above derivations, we have used the assumption that the boundary value of the coefficient  $\sigma_a$  is known, i.e.  $\delta\sigma_{a|\partial\Omega}=0$ ; see the assumption in  $(\mathcal{A}\text{-iv})$  and  $\delta\sigma_a\in\mathcal{C}^1_0(\Omega)$ .

We first observe from the simplified  $P_2$  model (9), following standard elliptic theory [28, 32, 47, 52], that for  $0 \le k \le 2$ ,

$$\|(\phi_{1,j},\phi_{2,j})\|_{[\mathcal{H}^k(\Omega)]^2} \le \mathfrak{c}_1 \|f_j\|_{L^2(\partial\Omega)}.$$

In the same way, equation (26) admits a unique solution with

$$\|(\widehat{\phi}_{1,j},\widehat{\phi}_{2,j})\|_{[\mathcal{H}^{k}(\Omega)]^{2}} \leq \mathfrak{c}_{2}\|\delta\sigma_{a}(\phi_{1,j},\phi_{2,j})\|_{[L^{2}(\Omega)]^{2}} \leq \widetilde{\mathfrak{c}}_{2}\|\delta\sigma_{a}\|_{\mathcal{C}_{0}^{1}(\Omega)}\|(\phi_{1,j},\phi_{2,j})\|_{[L^{2}(\Omega)]^{2}}, \tag{28}$$

while (27) admits a unique solution satisfying

$$\|(\overline{\overline{\phi}}_{1,j},\overline{\overline{\phi}}_{2,j})\|_{[\mathcal{H}^k(\Omega)]^2} \leq \mathfrak{c}_3 \|\delta\sigma_a(\widehat{\phi}_{1,j},\widehat{\phi}_{2,j})\|_{[L^2(\Omega)]^2} \leq \widetilde{\mathfrak{c}}_3 \|\delta\sigma_a\|_{\mathcal{C}_0^1(\Omega)} \|(\widehat{\phi}_{1,j},\widehat{\phi}_{2,j})\|_{[L^2(\Omega)]^2}. \tag{29}$$

We then deduce that

$$\|(\overline{\overline{\phi}}_{1,j}, \overline{\overline{\phi}}_{2,j})\|_{[\mathcal{H}^k(\Omega)]^2} \le \mathfrak{c}_4 \|\delta\sigma_a\|_{\mathcal{C}_0^1(\Omega)}^2 \|f_j\|_{L^2(\partial\Omega)},\tag{30}$$

which then leads to,

$$\lim_{\|\delta\sigma_a\|_{\mathcal{C}_0^1(\Omega)}\to 0} \frac{\|(\overline{\overline{\phi}}_{1,j},\overline{\overline{\phi}}_{2,j})\|_{[\mathcal{H}^k(\Omega)]^2}}{\|\delta\sigma_a\|_{\mathcal{C}_0^1(\Omega)}} \equiv \lim_{\|\delta\sigma_a\|_{\mathcal{C}_0^1(\Omega)}\to 0} \frac{\|(\widehat{\phi}_{1,j}-\widetilde{\phi}_{1,j},\widehat{\phi}_{2,j}-\widetilde{\phi}_{2,j})\|_{[\mathcal{H}^k(\Omega)]^2}}{\|\delta\sigma_a\|_{\mathcal{C}_0^1(\Omega)}} = 0. \quad (31)$$

This shows that  $(\phi_{1,j}, \phi_{2,j})$  is Fréchet differentiable with respect to  $\sigma_a$  as a map:  $\mathcal{C}^1(\overline{\Omega}) \mapsto \mathcal{H}^k(\Omega) \times \mathcal{H}^k(\Omega)$ ,  $0 \leq k \leq 2$ , with Fréchet derivative in direction  $\delta \sigma_a \in \mathcal{C}^1_0(\Omega)$  given by  $(\widetilde{\phi}_{1,j}, \widetilde{\phi}_{2,j})$ . Differentiability of  $H_j^{\mathcal{M}}$  with respect to  $\sigma_a$  then follows from this fact and the chain rule.

To compute the Fréchet derivative of  $\mathcal{O}(\sigma_a, \sigma_s)$  with respect to  $\sigma_a$ , we first compute

$$H_j^{\mathcal{M}'}(\sigma_a, \sigma_s)[\delta\sigma_a] = \Xi(\phi_{1,j} - \frac{2}{3}\phi_{2,j})\delta\sigma_a + \Xi\sigma_a(\phi_{1,j} - \frac{2}{3}\phi_{2,j})'(\sigma_a, \sigma_s)[\delta\sigma_a],$$

and

$$\mathcal{O}'(\sigma_a, \sigma_s)[\delta \sigma_a] = \sum_{j=1}^J \int_0^T \int_{\partial \Omega} (p_j^{\mathcal{M}} - p_j^*) p_j^{\mathcal{M}'}(\sigma_a, \sigma_s)[\delta \sigma_a] dS(\mathbf{x}) dt + \alpha \mathcal{R}'(\sigma_a)[\delta \sigma_a]. \tag{32}$$

Let us denote  $w_j := p_j^{\mathcal{M}'}(\sigma_a, \sigma_s)[\delta \sigma_a]$ . We verify that  $w_j$  solves

$$\frac{1}{c^{2}(\mathbf{x})} \frac{\partial^{2} w_{j}}{\partial t^{2}} - \Delta w_{j} = 0, \text{ in } \mathbb{R}_{+} \times \Omega$$

$$w_{j}(t, \mathbf{x}) = H_{j}^{\mathcal{M}'}(\sigma_{a}, \sigma_{s})[\delta \sigma_{a}], \quad \frac{\partial w_{j}}{\partial t}(t, \mathbf{x}) = 0, \text{ in } \{0\} \times \Omega$$

$$\mathbf{n} \cdot \nabla w_{j} = 0, \text{ on } \mathbb{R}_{+} \times \partial \Omega.$$
(33)

Multiplying the equation for  $q_j$ , (18), by  $w_j$ , the equation for  $w_j$ , (33), by  $q_j$ , and integrating the difference over  $(0,T) \times \Omega$ , we arrive at

$$\int_{0}^{T} \int_{\partial\Omega} (p_{j}^{\mathcal{M}} - p_{j}^{*}) w_{j} dS(\mathbf{x}) dt = \int_{\Omega} \frac{\Xi}{c^{2}} (\phi_{1,j} - \frac{2}{3}\phi_{2,j}) \frac{\partial q_{j}}{\partial t} (0, \mathbf{x}) \delta\sigma_{a} d\mathbf{x} 
+ \int_{\Omega} \frac{\Xi}{c^{2}} \sigma_{a} (\phi_{1,j} - \frac{2}{3}\phi_{2,j})' (\sigma_{a}, \sigma_{s}) [\delta\sigma_{a}] \frac{\partial q_{j}}{\partial t} (0, \mathbf{x}) d\mathbf{x}, \quad (34)$$

thanks to Green's theorem.

Multiplying the equation for  $(\psi_{1,j}, \psi_{2,j})$ , i.e. (21), by  $(\widetilde{\phi}_{1,j}, \widetilde{\phi}_{2,j})$  (which is nothing but  $(\phi'_{1,j}(\sigma_a, \sigma_s)[\delta\sigma_a], \phi'_{2,j}(\sigma_a, \sigma_s)[\delta\sigma_a])$ ), the equation for  $(\widetilde{\phi}_{1,j}, \widetilde{\phi}_{2,j})$ , i.e. (25), by  $(\psi_{1,j}, \psi_{2,j})$ , and integrating the difference over  $\Omega$ , we obtain

$$\int_{\Omega} \frac{\Xi}{c^2} \sigma_a(\phi_{1,j} - \frac{2}{3}\phi_{2,j})'(\sigma_a, \sigma_s) [\delta \sigma_a] \frac{\partial q_j}{\partial t}(0, \mathbf{x}) d\mathbf{x}$$

$$= \int_{\Omega} (\phi_{1,j} - \frac{2}{3}\phi_{2,j}) (\psi_{1,j} - \frac{2}{3\kappa}\psi_{2,j}) \delta \sigma_a d\mathbf{x}. \quad (35)$$

We now combine (32), (34) and (35) to get the final result in (19). Similar calculations for  $\sigma_s$  yield the result in (20). This completes the proof.

Let us emphasize here that the simplified  $P_2$  diffusion system (9) is not self-adjoint. Therefore, the diffusion operators and the boundary conditions in (21) are different from those in (9).

The calculations in Lemma 3.1 allow us to develop a subroutine for the SNOPT algorithm to evaluate the mismatch functional  $\mathcal{O}$  and its derivatives with respect to  $\sigma_a$  and  $\sigma_s$ . For the convenience of presentation, let us denote by  $\mathcal{O}_j(\sigma_a,\sigma_s)$  the contributions to the mismatch functional  $\mathcal{O}$  from source  $f_j$ , that is,  $\mathcal{O}_j(\sigma_a,\sigma_s)=\frac{1}{2}\int_0^T\int_{\partial\Omega}(p_j^{\mathcal{M}}-p_j^*)^2dS(\mathbf{x})dt$ . We use  $\mathcal{O}_j'$  to denote the derivative of  $\mathcal{O}_j$  at  $(\sigma_a,\sigma_s)$ . The algorithm for calculating  $\mathcal{O}$  and  $\mathcal{O}'$  is summarized in **Subroutine** 1.

#### Subroutine 1 Evaluating $\mathcal{O}$ and Its Derivatives at $(\sigma_a, \sigma_s)$ for Model $\mathcal{M}$

```
1: Initialize \mathcal{O} = 0 and \mathcal{O}' = \mathbf{0}
 2: for j = 1 to J do
            Solve the forward model \mathcal{M} (i.e., (9) or (12)), with illumination source f_i
 3:
            Evaluate initial pressure field H_j^{\mathcal{M}} for model \mathcal{M} (following (7) or (13))
Solve the wave equation (3) with initial condition H_j^{\mathcal{M}} for p_j^{\mathcal{M}}
 4:
 5:
            Evaluate the residual z_j^{\mathcal{M}} = p_j^{\mathcal{M}} - p_j^* and \mathcal{O}_j = \frac{1}{2} \int_0^T \int_{\partial\Omega} (z_j^{\mathcal{M}})^2 dS(\mathbf{x}) dt
 6:
             \mathcal{O} \leftarrow \mathcal{O} + \mathcal{O}_j
 7:
             Solve the adjoint wave equation (18), and evaluate \partial_t q_i(0, \mathbf{x})
 8:
             Solve the adjoint diffusion equation for model \mathcal{M} (i.e., (21) or (24))
 9:
10:
             Evaluate the derivative \mathcal{O}'_i (following (19) and (20), or (22) and (23))
             \mathcal{O}' \leftarrow \mathcal{O}' + \mathcal{O}'_i
11:
12: end for
13: \mathcal{O} \leftarrow \mathcal{O} + \alpha \mathcal{R}(\sigma_a) + \beta \mathcal{R}(\sigma_s)
14: \mathcal{O}' \leftarrow \mathcal{O}' + \alpha \mathcal{R}'(\sigma_a)[\delta \sigma_a] + \beta \mathcal{R}'(\sigma_s)[\delta \sigma_s]
```

# 4 Quantitative inversion with simplified $P_2$

The reconstruction algorithm we implemented in the previous section is based on the onestep approach: we reconstruct the optical coefficients directly from the measured ultrasound signal. This is the same approach that has been recently used in [25, 57, 63]. An alternative, in fact more popular, approach for PAT reconstruction is a two-step strategy: (i) to reconstruct the initial pressure field H from measured ultrasound data; and then (ii) to reconstruct the optical coefficients from the reconstructed initial pressure field H. The first step involves only the acoustic model and is independent of the optical model, and reconstruction algorithms for this step have previously been developed in many scenarios [2, 3, 4, 15, 17, 30, 36, 38, 44, 58, 68, 72, 76]. The second step of the reconstruction have been developed for both the diffusion model (12) [10, 12] and the radiative transport model (1) [9, 51, 64], but not the simplified  $P_2$  model (9), to our best knowledge.

The objective of this section is to study the quantitative step of PAT with the simplified  $P_2$  model: to reconstruct the optical coefficients from the initial pressure field data H that one recovers from the ultrasound measurements. We assume again that we have data generated from  $J \geq 1$  illumination sources. Let  $(\phi_{1,j}, \phi_{2,j})$  be the solution to the simplified  $P_2$  system (9) with source  $f_j$ . In the quantitative step, we wish to recover the optical coefficients from the data  $\{H_j^{P_2}\}_{j=1}^J$ .

The case of reconstructing  $\sigma_a$  only. We first consider the case where the absorption coefficient  $\sigma_a$  is the only coefficient to be reconstructed. That is, the Grüneisen coefficient and the scattering coefficient are both known. In this case, we can show that  $\sigma_a$  can be uniquely recovered from only one initial pressure field. Moreover, the reconstruction of  $\sigma_a$  is a relatively stable process.

**Theorem 4.1.** Under the assumptions in (A-i)-(A-iv) and (8), let  $H_j^{P_2}$  and  $\widetilde{H}_j^{P_2}$  be the

initial pressure field corresponding to the coefficients  $(\Xi, \sigma_a, \sigma_s)$  and  $(\Xi, \widetilde{\sigma}_a, \sigma_s)$  respectively, induced by illumination source  $f_j$ . Assume further that  $(\sigma_a, \widetilde{\sigma}_a) \in C^1(\overline{\Omega}) \times C^1(\overline{\Omega})$ , and  $f_j$  is such that the corresponding solution to the simplified  $P_2$  model satisfies the condition  $(\phi_{1,j} - \frac{2}{3}\phi_{2,j}) \neq 0$  a.e.. Then  $H_j^{P_2} = \widetilde{H}_j^{P_2}$  a.e. implies  $\sigma_a = \widetilde{\sigma}_a$  a.e.. Moreover, we have the stability estimate

$$\|(\sigma_a - \widetilde{\sigma}_a)(\phi_{1,j} - \frac{2}{3}\phi_{2,j})\|_{L^2(\Omega)} \le \mathfrak{c}\|H_j^{P_2} - \widetilde{H}_j^{P_2}\|_{L^2(\Omega)},\tag{36}$$

where the constant  $\mathfrak{c}$  depends on  $\Omega$ ,  $\Xi$ ,  $\sigma_s$ ,  $\underline{\alpha}$  and  $\overline{\alpha}$ .

*Proof.* Let  $\Phi_{i,j} = \phi_{i,j} - \widetilde{\phi}_{i,j}$ , i = 1, 2, where  $(\phi_{1,j}, \phi_{2,j})$  and  $(\widetilde{\phi}_{1,j}, \widetilde{\phi}_{2,j})$  are solutions to (9) with  $(\sigma_a, \sigma_s)$  and  $(\widetilde{\sigma}_a, \sigma_s)$  respectively. We verify that  $(\Phi_{1,j}, \Phi_{2,j})$  solves the following system

$$-\nabla \cdot D\nabla \Phi_{1,j} + \frac{H_{j}^{P_{2}} - \widetilde{H}_{j}^{P_{2}}}{\Xi} = 0, \text{ in } \Omega$$

$$-\nabla \cdot D\nabla \Phi_{2,j} + \frac{5}{9\kappa'} \frac{1}{D} \Phi_{2,j} - \frac{2}{3\kappa} \frac{H_{j}^{P_{2}} - \widetilde{H}_{j}^{P_{2}}}{\Xi} = 0, \text{ in } \Omega$$

$$\mathbf{n} \cdot D\nabla \Phi_{1,j} + \frac{1}{2} \Phi_{1,j} - \frac{1}{8} \Phi_{2,j} = 0, \text{ on } \partial\Omega$$

$$\mathbf{n} \cdot D\nabla \Phi_{2,j} + \frac{7}{24\kappa} \Phi_{2,j} - \frac{1}{8\kappa} \Phi_{1,j} = 0, \text{ on } \partial\Omega$$

$$(37)$$

The coefficients (i.e. D and  $\sigma_{a2}$ ) in this system of equations are all known (since  $\sigma_s$  is known), independent of the unknown absorption coefficient  $\sigma_a$ . With the regularity assumptions we have, standard elliptic theory [32, 52] shows that when  $H_j^{P_2} = \widetilde{H}_j^{P_2}$  a.e., i.e.  $H_j^{P_2} - \widetilde{H}_j^{P_2} = 0$  a.e., the solution  $(\Phi_{1,j}, \Phi_{2,j}) = (0,0)$  a.e.. This immediately implies that  $(\phi_{1,j}, \phi_{2,j}) = (\widetilde{\phi}_{1,j}, \widetilde{\phi}_{2,j})$ . Therefore,  $\sigma_a = \frac{H_j^{P_2}}{\phi_{1,j} - \frac{2}{3}\phi_{2,j}} = \widetilde{\sigma}_a$  if  $\phi_{1,j} - \frac{2}{3}\phi_{2,j} \neq 0$  a.e.. This proves the uniqueness part of the theorem.

To derive the stability estimate (36), we observe that

$$|\frac{H_{j}^{P_{2}} - \widetilde{H}_{j}^{P_{2}}}{\Xi}| = |\sigma_{a}(\phi_{1,j} - \frac{2}{3}\phi_{2,j}) - \widetilde{\sigma}_{a}(\widetilde{\phi}_{1,j} - \frac{2}{3}\widetilde{\phi}_{2,j})| = |(\sigma_{a} - \widetilde{\sigma}_{a})(\phi_{1,j} - \frac{2}{3}\phi_{2,j}) + \widetilde{\sigma}_{a}(\Phi_{1,j} - \frac{2}{3}\Phi_{2,j})|.$$

This, together with the triangle inequality, gives that

$$\|(\sigma_a - \widetilde{\sigma}_a)(\phi_{1,j} - \frac{2}{3}\phi_{2,j})\|_{L^2(\Omega)} \le \mathfrak{c}_1 \left| \frac{H_j^{P_2} - \widetilde{H}_j^{P_2}}{\Xi} \right|_{L^2(\Omega)} + \mathfrak{c}_2 \|(\Phi_j, \Psi_j)\|_{[L^2(\Omega)]^2}, \tag{38}$$

using the fact that  $\sigma_a$  and  $\widetilde{\sigma}_a$  are bounded as in the assumption ( $\mathcal{A}$ -ii).

On the other hand, the system (40) provides us with the following stability estimate for  $(\Phi_{1,j}, \Phi_{2,j})$ :

$$\|(\Phi_{1,j}, \Phi_{2,j})\|_{[\mathcal{H}^2(\Omega)]^2} \le \mathfrak{c}_3 \|H_j^{P_2} - \widetilde{H}_j^{P_2}\|_{L^2(\Omega)}. \tag{39}$$

The estimate (36) then follows by combining (38) and (39).

The above proof is constructive in the sense that it provides an explicit procedure for the reconstruction of  $\sigma_a$ . To do that, we first solve

$$-\nabla \cdot D\nabla \phi_{1,j} + \frac{H_j^{P_2}}{\Xi} = 0, \quad \text{in } \Omega$$

$$-\nabla \cdot D\nabla \phi_{2,j} + \frac{5}{9\kappa'} \frac{1}{D} \phi_{2,j} - \frac{2}{3\kappa} \frac{H_j^{P_2}}{\Xi} = 0, \quad \text{in } \Omega$$

$$\mathbf{n} \cdot D\nabla \phi_{1,j} + \frac{1}{2} \phi_{1,j} - \frac{1}{8} \phi_{2,j} = \frac{1}{2} f_j(\mathbf{x}), \quad \text{on } \partial\Omega$$

$$\mathbf{n} \cdot D\nabla \phi_{2,j} + \frac{7}{24\kappa} \phi_{2,j} - \frac{1}{8\kappa} \phi_{1,j} = -\frac{1}{8\kappa} f_j(\mathbf{x}), \quad \text{on } \partial\Omega$$

$$(40)$$

for  $(\phi_{1,j}, \phi_{2,j})$ . We then simply reconstruct the absorption coefficient as  $\sigma_a = \frac{H_j^{P_2}}{\Xi(\phi_{1,j} - \frac{2}{3}\phi_{2,j})}$  at points where  $\phi_{1,j}(\mathbf{x}) - \frac{2}{3}\phi_{2,j}(\mathbf{x}) \neq 0$ . When J data sets are available, we reconstruct  $\sigma_a$  as

$$\sigma_a = \frac{\sum_{j=1}^{J} H_j^{P_2}}{\Xi \sum_{j=1}^{J} (\phi_{1,j} - \frac{2}{3}\phi_{2,j})}.$$

Therefore, to reconstruct  $\sigma_a$  from J initial pressure fields, we only need to solve J diffusion systems (40) and perform some algebraic operations afterwards, even though the reconstruction problem is a nonlinear inverse problem.

The case of reconstructing the scattering coefficient or more than one coefficients are significantly more complicated, as demonstrated in the case of the classical diffusion model studied in [10, 12]. We do not have results for these cases in the full nonlinear setting. We will instead study the problem in the linearized setting.

We now use the second form of the simplified  $P_2$  system given in (10). We linearize the system formally following the differentiability result in Lemma 3.1. We use  $(\Xi, \sigma_a, \sigma_s)$  and  $(\delta\Xi, \delta\sigma_a, \delta\sigma_s)$  (note the equivalence  $\delta D = -\delta\sigma_s/[3(1-g)\sigma_s^2]$ ) to denote respectively the background coefficients and the perturbation to the coefficients. We use

$$(w_j, \phi_{2,j}) = (\phi_{1,j} - \frac{2}{3}\phi_{2,j}, \phi_{2,j}), \quad \text{and} \quad (\delta w_j, \delta \phi_{2,j}) = (\delta \phi_{1,j} - \frac{2}{3}\delta \phi_{2,j}, \delta \phi_{2,j})$$
 (41)

to denote the solutions to the background problem and the perturbations to the background solution caused by the perturbation in the coefficients, respectively. We then have that  $(w_j, \phi_{2,j})$  solves

$$-\nabla \cdot D\nabla w_{j} + (1 + \frac{4}{9\kappa})\sigma_{a}w_{j} - \frac{10}{27\kappa'D}\phi_{2,j} = 0, \quad \text{in } \Omega 
-\nabla \cdot D\nabla\phi_{2,j} + \frac{5}{9\kappa'D}\phi_{2,j} - \frac{2}{3\kappa}\sigma_{a}w_{j} = 0, \quad \text{in } \Omega 
\mathbf{n} \cdot D\nabla w_{j} + \frac{6\kappa+1}{12}w_{j} + \frac{15\kappa-10}{72\kappa}\phi_{2,j} = \frac{6\kappa+1}{12}f_{j}(\mathbf{x}), \quad \text{on } \partial\Omega 
\mathbf{n} \cdot D\nabla\phi_{2,j} + \frac{5}{24\kappa}\phi_{2,j} - \frac{1}{8\kappa}w_{j} = -\frac{1}{8\kappa}f_{j}(\mathbf{x}), \quad \text{on } \partial\Omega$$
(42)

while  $(\delta w_j, \delta \phi_{2,j})$  solves

$$-\nabla \cdot D\nabla \delta w_{j} + (1 + \frac{4}{9\kappa})\sigma_{a}\delta w_{j} - \frac{10}{27\kappa'D}\delta\phi_{2,j} = \nabla \cdot \delta D\nabla w_{j} - (1 + \frac{4}{9\kappa})w_{j}\delta\sigma_{a} - \frac{10}{27\kappa'D^{2}}\phi_{2,j}\delta D, \text{ in } \Omega$$

$$-\nabla \cdot D\nabla \delta\phi_{2,j} + \frac{5}{9\kappa'D}\delta\phi_{2,j} - \frac{2\sigma_{a}}{3\kappa}\delta w_{j} = \nabla \cdot \delta D\nabla\phi_{2,j} + \frac{5\phi_{2,j}}{9\kappa'D^{2}}\delta D + \frac{2w_{j}}{3\kappa}\delta\sigma_{a}, \text{ in } \Omega$$

$$\mathbf{n} \cdot D\nabla \delta w_{j} + \frac{6\kappa+1}{12}\delta w_{j} + \frac{15\kappa-10}{72\kappa}\delta\phi_{2,j} = 0, \text{ on } \partial\Omega$$

$$\mathbf{n} \cdot D\nabla \delta\phi_{2,j} + \frac{5}{24\kappa}\delta\phi_{2,j} - \frac{1}{8\kappa}\delta w_{j} = 0, \text{ on } \partial\Omega$$

$$(43)$$

where we have used the fact that  $D_{|\partial\Omega}$  is known (since  $\sigma_{s|\partial\Omega}$  is known) in the boundary conditions.

The perturbed initial pressure field, the data, now take the form:

$$\delta H_j^{P_2} = (\delta \Xi \sigma_a + \Xi \delta \sigma_a) w_j + \Xi \sigma_a \delta w_j. \tag{44}$$

The linearized data show that if the background Grüneisen coefficient  $\Xi=0$ , then  $\delta H_j^{P_2}=\delta\Xi\sigma_a(\phi_{1,j}-\frac{2}{3}\phi_{2,j})$ . Therefore, we can reconstruct  $\delta\Xi$ , but not the other parameters. If the background absorption coefficient  $\sigma_a=0$  (which means that the medium is weakly absorbing), then  $\delta H_j^{P_2}=\Xi\delta\sigma(\phi_{1,j}-\frac{2}{3}\phi_{2,j})$ . Therefore, we can reconstruct  $\delta\sigma_a$  but not the other parameters.

The case of reconstructing  $\sigma_s$  only. We start with the case of reconstructing only the scattering coefficient.

We have the following result in the linearized setting.

**Theorem 4.2.** Under the assumptions in (A-i)-(A-iv) and (8) for the domain and the background coefficients, let  $\delta H_j^{P_2}$  and  $\delta \widetilde{H}_j^{P_2}$  be two perturbed data sets generated with perturbed coefficients  $\delta \sigma_s$  and  $\delta \widetilde{\sigma}_s$  respectively. Then we have the following bound on the reconstruction:

$$\int_{\Omega} Q_j \left( \frac{\delta D}{D} - \frac{\delta \widetilde{D}}{D} \right)^2 d\mathbf{x} \le \mathfrak{c} \|\delta H_j^{P_2} - \delta \widetilde{H}_j^{P_2}\|_{\mathcal{H}^2(\Omega)}$$
(45)

where the constant  $\mathfrak{c}$  depends on  $\Omega$  and the background coefficients, and  $Q_j$  is defined as

$$Q_{j}(\mathbf{x}) := ((1 + \frac{4}{9\kappa})\sigma_{a}w_{j} - 4\gamma\phi_{2,j})\phi_{2,j} - \mathbf{u} \cdot \nabla\phi_{2,j} - \frac{1}{3}D|\nabla\phi_{2,j}|^{2}.$$
 (46)

If  $Q_j(\mathbf{x}) > -\frac{10}{27\kappa'D}\phi_{2,j}^2$  or  $Q_j(\mathbf{x}) \geq -\frac{10}{27\kappa'D}\phi_{2,j}^2$  and  $|\nabla w_j| \geq \varepsilon > 0$  for some  $\varepsilon$ , then  $\delta H_j^{P_2} = \delta \widetilde{H}_j^{P_2}$  a.e on  $\Omega$  implies  $\delta \sigma_s = \delta \widetilde{\sigma}_s$  a.e..

*Proof.* When only  $\sigma_s$  is sought, the perturbed datum (44) simplifies to

$$\frac{\delta H_j^{P_2}}{\Xi} = \sigma_a \delta w_j, \tag{47}$$

while the perturbed simplified  $P_2$  system (43) simplifies to

$$-\nabla \cdot D\nabla \delta w_{j} + (1 + \frac{4}{9\kappa})\sigma_{a}\delta w_{j} - \frac{10}{27\kappa'D}\delta\phi_{2,j} = \nabla \cdot \delta D\nabla w_{j} - \frac{10\phi_{2,j}}{27\kappa'D^{2}}\delta D, \text{ in } \Omega 
-\nabla \cdot D\nabla \delta\phi_{2,j} + \frac{5}{9\kappa'D}\delta\phi_{2,j} - \frac{2}{3\kappa}\sigma_{a}\delta w_{j} = \nabla \cdot \delta D\nabla\phi_{2,j} + \frac{5\phi_{2,j}}{9\kappa'D^{2}}\delta D, \text{ in } \Omega 
\mathbf{n} \cdot D\nabla \delta w_{j} + \frac{6\kappa+1}{12\kappa}\delta w_{j} + \frac{15\kappa-10}{72\kappa}\delta\phi_{2,j} = 0, \text{ on } \partial\Omega 
\mathbf{n} \cdot D\nabla \delta\phi_{2,j} + \frac{5}{24\kappa}\delta\phi_{2,j} - \frac{1}{8\kappa}\delta w_{j} = 0, \text{ on } \partial\Omega$$

$$(48)$$

Using (47), we can further rewrite (48) into

$$-\frac{10}{27\kappa'D}\delta\phi_{2,j} = \nabla \cdot \delta D \nabla w_{j} - \frac{10\phi_{2,j}}{27\kappa'D^{2}}\delta D + \nabla \cdot D \nabla \frac{\delta H_{j}^{P_{2}}}{\Xi\sigma_{a}} - \left(1 + \frac{4}{9\kappa}\right)\frac{\delta H_{j}^{P_{2}}}{\Xi}, \text{ in } \Omega$$

$$-\nabla \cdot D \nabla \delta\phi_{2,j} + \frac{5}{9\kappa'D}\delta\phi_{2,j} = \nabla \cdot \delta D \nabla\phi_{2,j} + \frac{5\phi_{2,j}}{9\kappa'D^{2}}\delta D + \frac{2}{3\kappa}\frac{\delta H_{j}^{P_{2}}}{\Xi}, \text{ in } \Omega$$

$$\mathbf{n} \cdot D \nabla \delta\phi_{2,j} + \frac{5}{24\kappa}\delta\phi_{2,j} = \frac{1}{8\kappa}\frac{\delta H_{j}^{P_{2}}}{\Xi\sigma_{a}}, \text{ on } \partial\Omega$$

$$\delta D = 0, \text{ on } \partial\Omega$$

Note that we have added the natural boundary condition for  $\delta D$  that we assumed in the assumption ( $\mathcal{A}$ -iv). This can now be seen as a system of partial differential equations with  $(\delta \phi_{2,i}, \delta D)$  as the unknown.

Let  $\mathbf{u} = D\nabla w_j$ ,  $\mu = \delta D/D$ ,  $\gamma = \frac{10}{27\kappa'D}$  and  $Y_j = \nabla \cdot D\nabla \frac{\delta H_j^{P_2}}{\Xi \sigma_a} - (1 + \frac{4}{9\kappa})\frac{\delta H_j^{P_2}}{\Xi}$ . We then verify that the first equation in (49) can be written as

$$\nabla \cdot \mu \mathbf{u} - \gamma \phi_{2,j} \mu + \gamma \delta \phi_{2,j} + Y_j = 0, \tag{50}$$

and the first equation in the background system (42) can be written as

$$-\nabla \cdot \mathbf{u} + \left(1 + \frac{4}{9\kappa}\right)\sigma_a w_j - \gamma \phi_{2,j} = 0.$$
 (51)

Moreover, we observe that for any scalar function  $\gamma$  and vector function  $\mathbf{u}$ , we have

$$\nabla \cdot \mu^2 \mathbf{u} - 2\mu \nabla \cdot \mu \mathbf{u} + \mu^2 \nabla \cdot \mathbf{u} = 0. \tag{52}$$

Using (50) and (51), we can write (52) as

$$\nabla \cdot \mu^{2} \mathbf{u} - \mu^{2} (3\gamma \phi_{2,j} - (1 + \frac{4}{9\kappa})\sigma_{a} w_{j}) + 2\mu (\gamma \delta \phi_{2,j} + Y_{j}) = 0.$$
 (53)

We multiply this equation by  $\phi_{2,j}$  and integrate over  $\Omega$  to get

$$\int_{\Omega} \mu^2 \left[ -\mathbf{u} \cdot \nabla \phi_{2,j} - (3\gamma \phi_{2,j} - (1 + \frac{4}{9\kappa})\sigma_a w_j)\phi_{2,j} \right] d\mathbf{x} + 2 \int_{\Omega} \mu(\gamma \delta \phi_{2,j} + Y_j)\phi_{2,j} d\mathbf{x} = 0.$$
 (54)

Meanwhile, we can multiply the second equation in (49) by  $\delta\phi_{2,j}$  and integrate over  $\Omega$  to get

$$\int_{\Omega} \left[ D|\nabla \delta \phi_{2,j}|^2 + \frac{3}{2}\gamma |\delta \phi_{2,j}|^2 + \mu D \nabla \phi_{2,j} \cdot \nabla \delta \phi_{2,j} - \frac{3}{2}\gamma \mu \phi_{2,j} \delta \phi_{2,j} - \frac{2}{3\kappa} \frac{\delta H_j^{P_2}}{\Xi} \delta \phi_{2,j} \right] d\mathbf{x} = 0.$$
(55)

We can now combine (54) and (55) to get

$$\int_{\Omega} \mu^{2} \left[ -\mathbf{u} \cdot \nabla \phi_{2,j} - (3\gamma \phi_{2,j} - (1 + \frac{4}{9\kappa})\sigma_{a}w_{j})\phi_{2,j} \right] d\mathbf{x} + \int_{\Omega} \left[ \frac{4}{3}D|\nabla \delta \phi_{2,j}|^{2} + 2\gamma|\delta \phi_{2,j}|^{2} \right] d\mathbf{x} 
+ \frac{4}{3} \int_{\Omega} \mu D\nabla \phi_{2,j} \cdot \nabla \delta \phi_{2,j} d\mathbf{x} + \int_{\Omega} 2\mu Y_{j}\phi_{2,j} d\mathbf{x} - \int_{\Omega} \frac{8}{9\kappa} \frac{\delta H_{j}^{P_{2}}}{\Xi} \delta \phi_{2,j} = 0. \quad (56)$$

Using the fact that  $\forall x, y \in \mathbb{R}$ ,  $xy \leq \frac{1}{2}((ax)^2 + (y/a)^2)$ ,  $\forall a \neq 0$ , we have the following bounds for the last three terms in above equation:

$$\int_{\Omega} \mu D \nabla \phi_{2,j} \cdot \nabla \delta \phi_{2,j} d\mathbf{x} \leq \int_{\Omega} \left[ \frac{1}{4} \mu^2 D |\nabla \phi_{2,j}|^2 + D |\nabla \delta \phi_{2,j}|^2 \right] d\mathbf{x},$$

$$\int_{\Omega} 2\mu Y_j \phi_{2,j} d\mathbf{x} \leq \int_{\Omega} \left[ \gamma \mu^2 \phi_{2,j}^2 + \frac{Y_j^2}{\gamma} \right] d\mathbf{x}, \quad \int_{\Omega} \frac{8\delta H_j^{P_2}}{9\kappa \Xi} \delta \phi_{2,j} \leq \int_{\Omega} \left[ (\frac{2\sqrt{2}\delta H_j^{P_2}}{9\kappa \Xi \sqrt{\gamma}})^2 + 2\gamma \delta \phi_{2,j}^2 \right] d\mathbf{x}.$$

These bounds can be combined with (56) to conclude that

$$\int_{\Omega} \mu^{2} \left[ ((1 + \frac{4}{9\kappa})\sigma_{a}w_{j} - 4\gamma\phi_{2,j})\phi_{2,j} - \mathbf{u} \cdot \nabla\phi_{2,j} - \frac{1}{3}D|\nabla\phi_{2,j}|^{2} \right] d\mathbf{x} \le \mathfrak{c} \|\delta H_{j}^{P_{2}}\|_{\mathcal{H}^{2}(\Omega)}^{2}, \quad (57)$$

with  $\mathfrak{c}$  depending on the background coefficients as well as  $\Omega$ . The stability result in (45) then follows from the linearity of the problem.

To prove the uniqueness claim, we observe that when  $\delta H_j^{P_2} = 0$  in (56), (57) becomes

$$\int_{\Omega} \left\{ \mu^2 \left[ Q_j + \gamma \phi_{2,j}^2 \right] + \gamma |\delta \phi_{2,j}|^2 \right\} d\mathbf{x} \le 0.$$
 (58)

When  $Q_j > -\gamma \phi_{2,j}^2$ , we conclude that  $\mu \equiv 0 \equiv \delta \phi_{2,j}$  from the above inequality. When  $Q_j + \gamma \phi_{2,j}^2 = 0$ , we conclude from the above inequality that  $\delta \phi_{2,j} \equiv 0$ . The first equation in (49) then simplifies to, with  $(\delta \phi_{2,j}, \delta H_j^{P_2}) = (0,0)$ ,

$$\nabla \cdot \mu \mathbf{u} - \gamma \phi_{2,j} \mu = 0$$
, in  $\Omega$ ,  $\mu = 0$ , on  $\partial \Omega$ .

This transport equation admits the unique solution  $\mu = 0$  when  $|\mathbf{u}| \geq \varepsilon > 0$  for some  $\varepsilon$  [10, 26]. The proof is complete.

We now consider the case where more than one coefficient is to be reconstructed. We focus on the practically important cases of reconstructing  $(\delta\Xi, \delta\sigma_a)$  and  $(\delta\sigma_a, \delta\sigma_s)$ .

The case of reconstructing  $(\delta\Xi, \delta\sigma_a)$ . In this case, the scattering coefficient  $\sigma_s$  (and therefore D) is known. Therefore the linearized simplified  $P_2$  equation (43) reduces to:

$$-\nabla \cdot D\nabla \delta w_{j} + (1 + \frac{4}{9\kappa})\sigma_{a}\delta w_{j} - \frac{10}{27\kappa'D}\delta\phi_{2,j} = -(1 + \frac{4}{9\kappa})\delta\sigma_{a}w_{j}, \text{ in } \Omega 
-\nabla \cdot D\nabla \delta\phi_{2,j} + \frac{5}{9\kappa'}\frac{1}{D}\delta\phi_{2,j} - \frac{2}{3\kappa}\sigma_{a}\delta w_{j} = \frac{2}{3\kappa}\delta\sigma_{a}w_{j}, \text{ in } \Omega 
\mathbf{n} \cdot D\nabla \delta w_{j} + \frac{6\kappa+1}{12}\delta w_{j} + \frac{15\kappa-10}{72\kappa}\delta\phi_{2,j} = 0, \text{ on } \partial\Omega 
\mathbf{n} \cdot D\nabla \delta\phi_{2,j} + \frac{5}{24\kappa}\delta\phi_{2,j} - \frac{1}{8\kappa}\delta w_{j} = 0, \text{ on } \partial\Omega$$
(59)

Since the linearized data (44) does not depend on the scattering coefficient  $\sigma_s$  explicitly, it remains in the original form in this case.

We now develop a two-stage procedure for the reconstruction of  $(\delta\Xi, \delta\sigma_a)$ . We first eliminate  $\delta\Xi$  from the system to reconstruct  $\delta\sigma_a$ . To do that, we check that, for any  $i \neq j$ ,

$$\delta H_{ij}^{P_2} \equiv w_j \frac{\delta H_i^{P_2}}{\Xi \sigma_a} - w_i \frac{\delta H_j^{P_2}}{\Xi \sigma_a} = w_j \delta w_i - w_i \delta w_j, \tag{60}$$

We then observe that  $\delta H_{ij}^{P_2}$  does NOT depend explicitly on the coefficient perturbation  $\delta\Xi$ . Moreover, the equations for the perturbations in (59) depend only on  $\delta\sigma_a$ . We could hope to reconstruct  $\delta\sigma_a$  out of (59) and (60).

We have the following partial result on the reconstruction of  $\delta \sigma_a$ .

**Theorem 4.3.** Under the assumptions in (A-i)-(A-iv) and (8), let  $\delta w_j$  and  $\delta w_j$  be solutions to (59) with coefficients  $\delta \sigma_a$  and  $\widetilde{\delta \sigma_a}$  respectively. Assume further that the illumination source  $f_j$  is selected such that the background solution  $w_j \neq 0$ . Then  $\delta w_j = \widetilde{\delta w_j}$  a.e. implies that  $\delta \sigma_a = \widetilde{\delta \sigma_a}$  a.e. . Moreover, we have the following stability bound:

$$\mathfrak{c}\|\delta w_j - \widetilde{\delta w_j}\|_{\mathcal{H}^2(\Omega)} \le \|(\delta \sigma_a - \widetilde{\delta \sigma}_a)w_j\|_{L^2(\Omega)} \le \widetilde{\mathfrak{c}}\|\delta w_j - \widetilde{\delta w_j}\|_{\mathcal{H}^2(\Omega)},\tag{61}$$

where  $\mathfrak{c}$  and  $\tilde{\mathfrak{c}}$  are constants that depend on the domain  $\Omega$ , the background coefficients and the background solution  $(w_i, \phi_{2,j})$ .

*Proof.* We first prove the injectivity claim. Let  $\delta w_j = 0$ . Then the first equation in (59) implies that

$$\delta \sigma_a w_j = \frac{10}{27\kappa' D} \delta \phi_{2,j} / (1 + \frac{4}{9\kappa}).$$

The second equation in (59), together with its boundary condition, then simplifies to

$$\begin{array}{rcl} -\nabla \cdot D\nabla \delta \phi_{2,j} + \kappa''' \delta \phi_{2,j} &=& 0, & \text{in } \Omega \\ \mathbf{n} \cdot D\nabla \delta \phi_{2,j} + \frac{5}{24\kappa} \delta \phi_{2,j} &=& 0, & \text{on } \partial \Omega \end{array}$$

where  $k''' = \frac{5}{9\kappa'} \frac{1}{D} - \frac{2}{3\kappa} \frac{10}{27\kappa'D} / (1 + \frac{4}{9\kappa})) > 0$ . This equation admits only the trivial solution  $\delta\phi_{2,j} \equiv 0$ . Therefore  $\delta\sigma_a \equiv 0$ .

To derive the stability bound (61), we first observe that the left inequality follows directly from classical theory for elliptic systems [32, 52]. To obtain the right inequality, we use the first equation in (59). We take the square of both sides of the equation, integrate over  $\Omega$ , and use the triangle and the Hölder's inequalities to obtain

$$\|\delta\sigma_a w_j\|_{L^2(\Omega)}^2 \le \mathfrak{c}_1 \left( \|\delta w_j\|_{\mathcal{H}^2}^2 + \|\delta\phi_{2,j}\|_{L^2(\Omega)}^2 + \|\delta w_j\|_{\mathcal{H}^1(\Omega)} \|\delta\phi_{2,j}\|_{L^2(\Omega)} \right). \tag{62}$$

We now multiply the first equation in (59) by  $\frac{2}{3\kappa}$ , the second equation by  $1 + \frac{4}{9\kappa}$ , and add the results together to get, after eliminating the factor  $1 + \frac{4}{9\kappa}$ ,

$$-\nabla \cdot D\nabla \delta \phi_{2,j} + \frac{5\kappa}{(4+9\kappa)\kappa' D} \delta \phi_{2,j} = \frac{6}{4+9\kappa} \nabla \cdot D\nabla \delta w_j, \text{ in } \Omega.$$
 (63)

Moreover, from the boundary condition for  $\delta \phi_{2,j}$  in (59) we have

$$\mathbf{n} \cdot D\nabla \delta \phi_{2,j} + \frac{5}{24\kappa} \delta \phi_{2,j} = \frac{1}{8\kappa} \delta w_j, \text{ on } \partial \Omega$$
 (64)

We can therefore look at (63) and (64) as an elliptic equation for  $\delta \phi_{2,j}$  and conclude from classical theory [32, 28] that

$$\|\delta\phi_{2,j}\|_{\mathcal{H}^2(\Omega)} \le \mathfrak{c}_2 \|\nabla \cdot D\nabla \delta w_j\|_{L^2(\Omega)} + \|\delta w_j\|_{L^2(\partial\Omega)} \le \tilde{\mathfrak{c}} \|\delta w_j\|_{\mathcal{H}^2(\Omega)}. \tag{65}$$

We now combine (62) and (65) to get the right equality in (61).

So long as we could select two illumination sources  $f_i$  and  $f_j$  such that the background densities  $w_i$  and  $w_j$  do not destroy the invertibility of the map  $\delta \sigma_a \mapsto \delta H_{ij}^{P_2} = w_i \delta w_j - w_j \delta w_i$ , note again that both  $\delta \sigma_a \mapsto \delta w_i$  and  $\delta \sigma_a \mapsto \delta w_j$  are invertible by the previous theorem, we could uniquely reconstruct  $\delta \sigma_a$  from  $\delta H_{ij}^{P_2}$ .

To perform numerical reconstruction of  $\delta \sigma_a$  from J data sets, we use the usual least-square inversion method. We minimize the functional

$$\Psi(\delta\sigma_a) = \sum_{1 \le i < j \le J} \|w_i \delta w_j - w_j \delta w_i - \delta H_{ij}^{P_2*}\|_{L_2(\Omega)}^2 + \beta \|\nabla \delta\sigma_a\|_{[L_2(\Omega)]^3}^2.$$
 (66)

Note that here we form the difference data using all (i, j) pairs satisfying i < j. There are totally J(J-1)/2 such pairs. We solve this minimization problem using the SNOPT algorithm we described in the previous section, even though this problem is linear. Once we reconstructed  $\delta \sigma_a$ , we can reconstruct  $\delta \Xi$  using the data (44):

$$\delta\Xi = \frac{\sum_{j=1}^{J} \delta H_j^{P_2} - \Xi \delta \sigma_a \sum_{j=1}^{J} w_j - \Xi \sigma_a \sum_{j=1}^{J} \delta w_j}{\sigma_a \sum_{j=1}^{J} w_j}.$$

The case of reconstructing  $(\delta \sigma_a, \delta \sigma_s)$ . In the case where  $\Xi$  is assumed known, the perturbed data (44) simplify to

$$\frac{\delta H_j^{P_2}}{\Xi} = \sigma_a \delta w_j + \delta \sigma_a w_j. \tag{67}$$

This simplification allows us to rewrite the system of equations for the perturbations, that is, system (43), into the form

$$-\nabla \cdot D\nabla \delta w_{j} - \frac{10}{27\kappa'D}\delta \phi_{2,j} = \nabla \cdot \delta D\nabla w_{j} - \frac{10\phi_{2,j}}{27\kappa'D^{2}}\delta D - \frac{9\kappa+4}{9\kappa}\frac{\delta H_{j}^{P_{2}}}{\Xi}, \text{ in } \Omega$$

$$-\nabla \cdot D\nabla \delta \phi_{2,j} + \frac{5}{9\kappa'D}\delta \phi_{2,j} = \nabla \cdot \delta D\nabla \phi_{2,j} + \frac{5\phi_{2,j}}{9\kappa'D^{2}}\delta D + \frac{2}{3\kappa}\frac{\delta H_{j}^{P_{2}}}{\Xi}, \text{ in } \Omega$$

$$\mathbf{n} \cdot D\nabla \delta w_{j} + \frac{6\kappa+1}{12}\delta w_{j} + \frac{15\kappa-10}{72\kappa}\delta \phi_{2,j} = 0, \text{ on } \partial \Omega$$

$$\mathbf{n} \cdot D\nabla \delta \phi_{2,j} + \frac{5}{24\kappa}\delta \phi_{2,j} - \frac{1}{8\kappa}\delta w_{j} = 0, \text{ on } \partial \Omega$$

$$(68)$$

This system does not depend explicitly on  $\delta \sigma_a$ .

The simplification (67) also allows us to form the difference data  $\delta H_{ij}^{P_2}$  in the same way as in (60). The difference data  $\delta H_{ij}^{P_2}$  in (60) do not depend on  $\delta \sigma_a$  either.

Let us again consider a two-stage procedure for the reconstruction of  $(\delta \sigma_a, \delta \sigma_s)$ . We first use the combination of (68) and (60) to reconstruct the perturbation of the scattering coefficient,  $\delta \sigma_s$  (or equivalently  $\delta D$ ). We then reconstruct  $\delta \sigma_a$  once  $\delta D$  has been reconstructed.

The following result is a simple corollary of Theorem 4.2.

Corollary 4.4. Under the same assumptions made in Theorem 4.2, the linear map

$$(\delta H_j^p, \delta w_j): \begin{array}{c} \delta \sigma_s \mapsto (\delta H_j^p, \delta w_j) \\ L^2(\Omega) \mapsto \mathcal{H}^2(\Omega) \times \mathcal{H}^2(\Omega) \end{array}$$

is injective when  $Q_j(\mathbf{x}) > -\frac{10}{27\kappa'D}\phi_{2,j}^2$  or  $Q_j(\mathbf{x}) \geq -\frac{10}{27\kappa'D}\phi_{2,j}^2$  and  $|\nabla w_j| \geq \varepsilon > 0$  for some  $\varepsilon$ . Moreover, we have the following stability bound:

$$\int_{\Omega} (\delta \sigma_s - \widetilde{\delta \sigma}_s)^2 Q_j d\mathbf{x} \le \mathfrak{c} \left( \|\delta H_j^{P_2} - \delta \widetilde{H}_j^{P_2}\|_{L^2(\Omega)}^2 + \|\delta w_j - \delta \widetilde{w}_j\|_{\mathcal{H}^2(\Omega)}^2 \right), \tag{69}$$

where  $\mathfrak{c}$  is a constant that depends on  $\Omega$  and the background coefficients.

*Proof.* The proof is almost identical to that of Theorem 4.2. If we move the terms involving  $\delta w_j$  to the right hand side, the system (68) has exactly the same structure as (48). The stability bound (69) follows from the same argument for (45). The injectivity claim follows when taking  $(\delta H_i^{P_2}, \delta w_j) = (0, 0)$ .

To reconstruct  $\delta D$  from data  $(\delta H_i^{P_2}, \delta H_{ij}^{P_2})$  (or equivalently  $(\delta H_i^{P_2}, \delta H_j^{P_2})$ ), we need to select two illumination sources  $f_i$  and  $f_j$  such that the background densities  $w_i$  and  $w_j$  do not destroy the injectivity of the map  $\delta D \mapsto (\delta H_i^{P_2}, \delta H_{ij}^{P_2}) = (\delta H_i^{P_2}, w_i \delta w_j - w_j \delta w_i)$ . Computationally, we solve the reconstruction problem by solving a least-square minimization problem with the same objective function in (66) (besides the regularization term which is now on  $\delta D$ ). Once we reconstructed  $\delta \sigma_a$ , we can reconstruct  $\delta \sigma_a$  using the data (67):

$$\delta \sigma_a = \frac{\sum_{j=1}^{J} \delta H_j^{P_2} / \Xi - \sigma_a \sum_{j=1}^{J} \delta w_j}{\sum_{j=1}^{J} w_j}.$$

Comparing simplified  $P_2$  and  $P_1$  reconstructions. The main motivation for using more accurate forward light propagation models in PAT is that the reconstructions based these models are more accurate. For instance, the difference between the reconstruction of the Grüneisen coefficient from the radiative transfer model (1) and that from the classical diffusion model (12), using the same data H, is given as

$$\Xi_{rte} - \Xi_{diff} = \frac{H(\varphi - \int_{\mathbb{S}^2} u(\mathbf{x}, \mathbf{v}) d\mathbf{v})}{\sigma_a(\int_{\mathbb{S}^2} u(\mathbf{x}, \mathbf{v}) d\mathbf{v}) \varphi(\mathbf{x})}$$

In this simple case, the error in the reconstruction of  $\Xi$  is proportional to the difference between the solutions to the two models. In the next theorem, we characterize the difference between the reconstruction of  $\sigma_a$  using the simplified  $P_2$  model (9) and that using the classical diffusion model (12).

**Theorem 4.5.** Let  $\Omega$ , c and  $\Xi$  satisfy the assumptions in (A-i)-(A-iv) and assume that the assumptions in (8) holds. Let  $\sigma_a^{P_2}$  and  $\sigma_a^{P_1}$  be the absorption coefficients reconstructed with the simplified  $P_2$  model (9) and the classical diffusion model (12) respectively, using the same datum H. Assume that H is also known on the boundary  $\partial\Omega$ . Then we have

$$\sigma_a^{P_2} - \sigma_a^{P_1} = \frac{H}{\Xi} \frac{\phi - (\phi_1 - \frac{2}{3}\phi_2)}{\phi(\phi_1 - \frac{2}{2}\phi_2)} = \frac{2}{3} \frac{\Xi}{H\sigma_a^{P_2}\sigma_a^{P_1}} \phi_2 \tag{70}$$

where  $\phi_2$  solves

$$-\nabla \cdot D\nabla \phi_2 + \frac{5}{9\kappa' D}\phi_2 = \frac{2}{3\kappa} \frac{H}{\Xi}, \quad in \Omega$$

$$\mathbf{n} \cdot D\nabla \phi_2 + \frac{5}{24\kappa}\phi_2 = \frac{1}{8\kappa} (\frac{H}{\sigma_a \Xi} - f(\mathbf{x})), \quad on \partial\Omega$$
(71)

*Proof.* We first observe that  $\sigma_a^{P_2}$  and  $\sigma_a^{P_1}$  can be explicitly reconstructed with the following procedures:

$$\sigma_a^{P_2} = \frac{H}{\Xi(\phi_1 - \frac{2}{3}\phi_2)} \quad \text{and} \quad \sigma_a^{P_1} = \frac{H}{\Xi\phi}$$
 (72)

where  $(\phi_1, \phi_2)$  is the solution to the simplified  $P_2$  system (9) with  $\sigma_a(\phi_1 - \frac{2}{3}\phi_2)$  replaced with  $H/\Xi$ , and  $\phi$  is the solution to the diffusion model (12) with  $\sigma_a\phi$  replaced by  $H/\Xi$ . In other words,  $(\phi_1, \phi_2)$  solves

$$-\nabla \cdot D\nabla \phi_{1} = -\frac{H}{\Xi}, \quad \text{in } \Omega$$

$$-\nabla \cdot D\nabla \phi_{2} + \frac{5}{9\kappa' D}\phi_{2} = \frac{2}{3\kappa}\frac{H}{\Xi}, \quad \text{in } \Omega$$

$$\mathbf{n} \cdot D\nabla \phi_{1} + \frac{5}{16}\phi_{1} = \frac{1}{2}f(\mathbf{x}) - \frac{3}{16}\frac{H}{\sigma_{a}\Xi}, \quad \text{on } \partial\Omega$$

$$\mathbf{n} \cdot D\nabla \phi_{2} + \frac{5}{24\kappa}\phi_{2} = \frac{1}{8\kappa}(\frac{H}{\sigma_{a}\Xi} - f(\mathbf{x})), \quad \text{on } \partial\Omega$$

$$(73)$$

while  $\phi$  solves

$$-\nabla \cdot D\nabla \phi = -\frac{H}{\Xi}, \quad \text{in } \Omega$$
  
$$\mathbf{n} \cdot D\nabla \phi + \frac{1}{2}\phi = \frac{1}{2}f(\mathbf{x}), \quad \text{on } \partial\Omega$$
 (74)

We therefore conclude that

$$\sigma_a^{P_2} - \sigma_a^{P_1} = \frac{H}{\Xi} \frac{\phi - (\phi_1 - \frac{2}{3}\phi_2)}{\phi(\phi_1 - \frac{2}{3}\phi_2)} = \frac{\Xi}{H\sigma_a^{P_2}\sigma_a^{P_1}} \left( (\phi - \phi_1) + \frac{2}{3}\phi_2 \right). \tag{75}$$

We observe from the second equation and its boundary condition (i.e. the forth equation) in (73) that  $\phi_2$  is the unique solution to (71).

Let  $\widetilde{\phi} = \phi - \phi_1$ . We verify that  $\widetilde{\phi}$  solves

$$-\nabla \cdot D\nabla \widetilde{\phi} = 0, \text{ in } \Omega$$

$$\mathbf{n} \cdot D\nabla \widetilde{\phi} + \frac{5}{16\kappa} \widetilde{\phi} = 0, \text{ on } \partial \Omega$$
(76)

where we have used the assumption that  $\sigma_a$  is known on  $\partial\Omega$ , made in (A-iv), so that  $(\phi_1 - \frac{2}{3}\phi_2) = \phi = \frac{H}{\Xi\sigma_a}$  on the boundary. This equation has a unique solution  $\widetilde{\phi} = 0$ . Therefore (75) simplifies to (70).

This result says that the difference between reconstructions based on the simplified  $P_2$  model (9) and reconstructions based on the classical diffusion model (12) are noticeable. In particular, if the data are generated with the simplified diffusion model (9), then using the classical diffusion model (12) would give us reconstructions that are simply not as accurate, vice versa. An implication of this is that if we believe that the data we used in PAT are generated by a physical process best modeled by the radiative transport equation (1), then using the simplified  $P_2$  model to perform reconstructions is advantageous to using the classical diffusion model, although we do not have an explicit characterization as in Theorem 4.5.

# 5 Numerical experiments

We now present some numerical simulations on the inverse problems studied in the previous sections. For simplicity, we consider a setup in which the physical properties and the illuminations used are invariant in the z direction so that we can perform simulations in the two-dimensional case.

The spatial variables in the simplified  $P_2$  model (9), the classical diffusion model (12), and the acoustic equation for ultrasound propagation (3) are discretized using the finite element method with piecewise linear Lagrange elements. The time variable in the wave equation is discretized with a second-order finite difference scheme. The optical illumination sources are all selected to have strength distribution along the boundary following the Gaussian distribution with standard deviation 0.5. The specific locations, i.e. centers, of the sources will be given later in the numerical examples.

The synthetic acoustic data we will use are generated by solving the forward diffusion models with the true optical properties and then feeding the corresponding initial pressure field H into the acoustic wave equation. To mimic measurement error, we pollute the data with additional random noise by multiplying each datum point by  $(1 + \sqrt{3}\eta \times 10^{-2} \text{random})$ , with random a uniformly distributed random variable taking values in [-1, 1], and  $\eta$  being the noise level (i.e. the size of the variance in percentage). When no additional random noise are added to the synthetic data, we will say the data are "clean"  $(\eta = 0)$ . Otherwise, we say the data are "noisy"  $(\eta \neq 0)$ .

The numerical simulations performed are all based on the minimization of the mismatch functional (15) as documented in Section 3. In all the simulations, the Grüneisen coefficient is assumed known and  $\Xi = 0.5$ . We emphasize that as long as  $\Xi$  is assumed known, whether or not it is a constant has no visible impact on the reconstruction of  $\sigma_a$  and  $\sigma_s$ .

We perform two groups of numerical simulations.

#### 5.1 Inversions based on the simplified $P_2$ model

In the first group, we study PAT reconstructions with the simplified  $P_2$  light propagation model. That is, we generate synthetic data using the model equation system (9) and perform

the reconstruction using the same system of equation.

Experiment 1 [Reconstructing  $\sigma_a$  from Acoustic Data]. In the first numerical experiment, we attempt to reconstruct the absorption coefficient assuming that the scattering coefficient, as well as the Grüneisen coefficient which is set to be  $\Xi = 0.5$  as mentioned above, is known. More precisely, the spatial domain we take is the square  $\Omega = (0, 2) \times (0, 2)$ , the scattering coefficient  $\sigma_s = 80$ , and the anisotropic factor of the scattering kernel g = 0.9. The true absorption coefficient has the form

$$\sigma_a(\mathbf{x}) = 0.1 + 0.1\chi_{B_1} + 0.2\chi_{B_2},\tag{77}$$

with  $B_1 = \{(x, y) : (x-1.0)^2 + (y-1.5)^2 \le (0.2)^2\}$  and  $B_2 = \{(x, y) : (x-1.5)^2 + (y-1.0)^2 \le (0.3)^2\}$ .

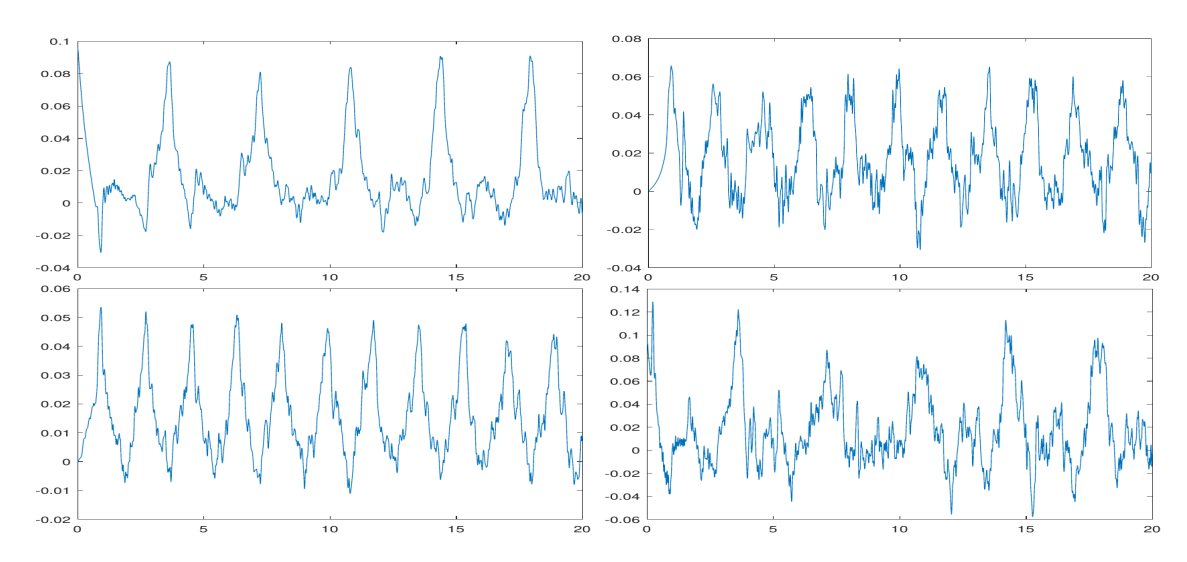


Figure 1: Ultrasound signals measured at two different locations ((0.0, 0.8) (left) and (1.0, 1.2) (right)) for two different illumination sources (top row: source located on the left boundary; bottom row: source located on the right boundary) in the time window (0, 20).

We first show in Figure 1 some typical acoustic signals we recorded in this setup. Shown are signals measured at (0.0, 0.8) and (1.0, 1.2) respectively for two different optical illuminations in the time interval (0, T = 20). Note that the data used in the reconstructions in the rest of the paper are on a larger time interval with T = 40, even though we observe in our numerical experiments that T = 10 is often more than enough for stable reconstructions.

In Figure 2, we show the reconstruction of the absorption coefficient (77) using data with noise levels  $\eta = 0$  (i.e. noise-free data) and  $\eta = 5$  respectively. The algorithm parameters are as follows. The initial guess for all the reconstructions is  $\sigma_a^0 = 0.1$ . The linear bounds we impose on the absorption coefficient are very loose:  $10^{-3} \le \sigma_a \le 0.5$ . The regularization parameter in (15) was chosen as  $\alpha = 1e - 9$  by trial and error.

Visual observation confirms that the reconstructions are of very high quality in this case, comparable to the quality of reconstructions for PAT using the radiative transfer model [22,

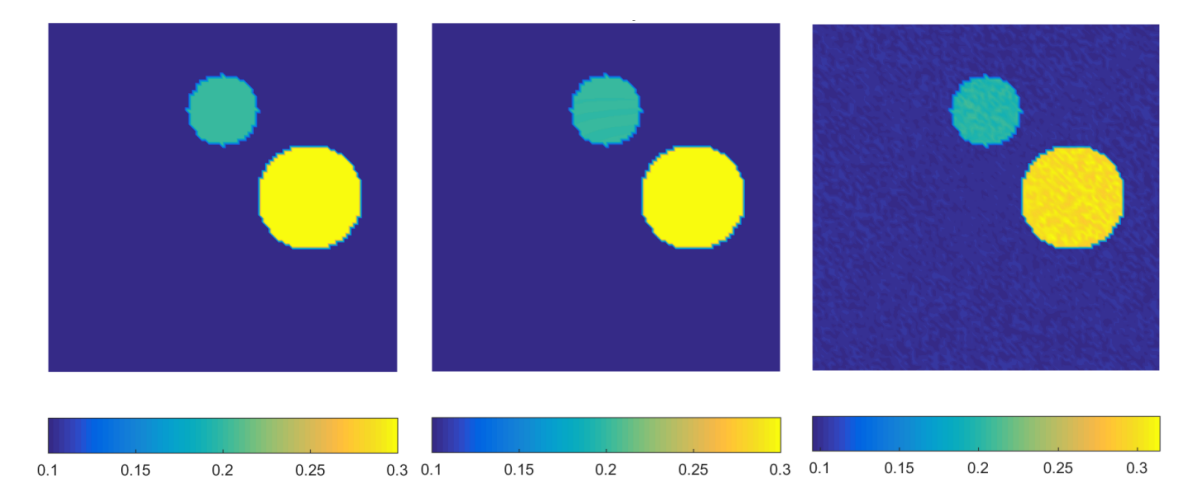


Figure 2: The absorption coefficient  $\sigma_a$  in (77) (left) and the reconstructions using noise-free data ( $\eta = 0$ , middle) and noisy data ( $\eta = 5$ , right).

51, 66] and the classic diffusion model [10, 19]. To quantitatively measure the quality of the reconstructions, we compute the relative  $L^2$  distance between the reconstructions and the true coefficient. This distance is defined as

$$\mathcal{E} = \frac{\|\hat{\sigma}_a - \sigma_a\|_{L^2(\Omega)}}{\|\sigma_a\|_{L^2(\Omega)}},$$

where  $\sigma_a$  and  $\hat{\sigma}_a$  are respectively the true and reconstructed absorption coefficients. The relative  $L^2$  error for the reconstructions in Figure 2 are respectively  $\mathcal{E} = 0.006$  and  $\mathcal{E} = 0.035$  for the case of  $\eta = 0$  and  $\eta = 5$ . The reconstruction results are very stable with respect to the initial guess we used, and the linear bounds we imposed on  $\sigma_a$  do not play a major role in this case either. These observations indicate that the inverse problem is fairly well-conditioned.

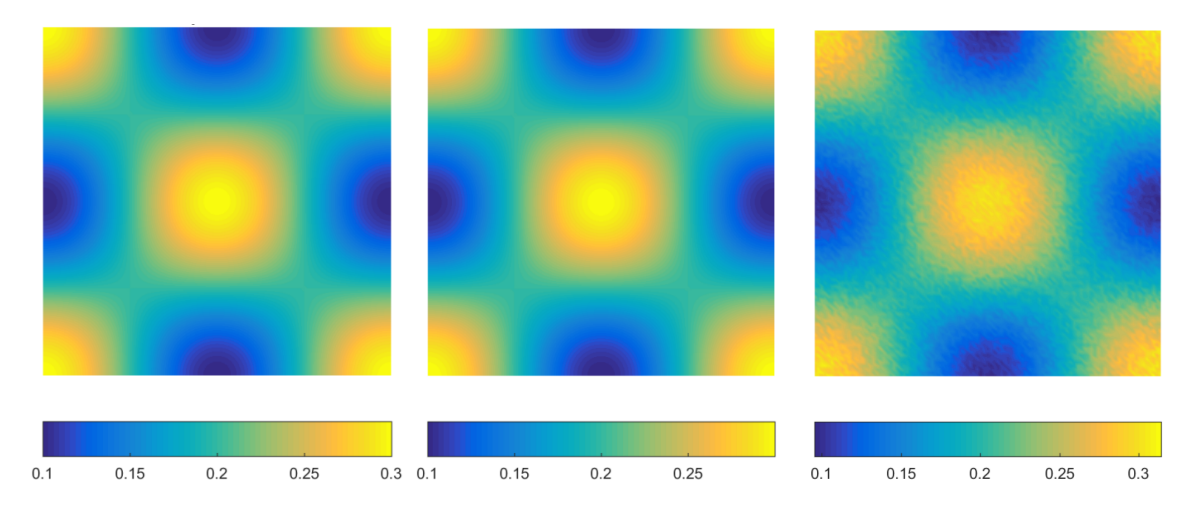


Figure 3: The absorption coefficient  $\sigma_a$  in (78) (left) and the reconstructions using noise-free data ( $\eta = 0$ , middle) and noisy data ( $\eta = 5$ , right).

We repeat similar numerical experiments for a few other absorption coefficients. The quality of the reconstruction results are very similar to the case we reported above. For

instance, in Figure 3, we show the reconstructions of a smooth absorption map defined as

$$\sigma_a(\mathbf{x}) = 0.2 + 0.1\cos(\pi x - \pi)\cos(\pi y - \pi).$$
 (78)

We again used the four sources to generate four data sets and initialize the reconstruction algorithm at  $\sigma_a^0 = 0.1$ , very different from the true coefficient. We also impose the same pointwise inequality constraints on the absorption coefficient, i.e.  $10^{-3} \le \sigma_a \le 0.5$ , and the same regularization parameter  $\alpha$ . The reconstruction quality is comparable to the smooth case and with results from the diffusion model [19]. The reconstruction errors are concentrated at the discontinuities, as expected. The relative  $L^2$  error in the reconstructions are respectively  $\mathcal{E} = 0.004$  and  $\mathcal{E} = 0.034$  for the cases of  $\eta = 0$  and  $\eta = 5$ .

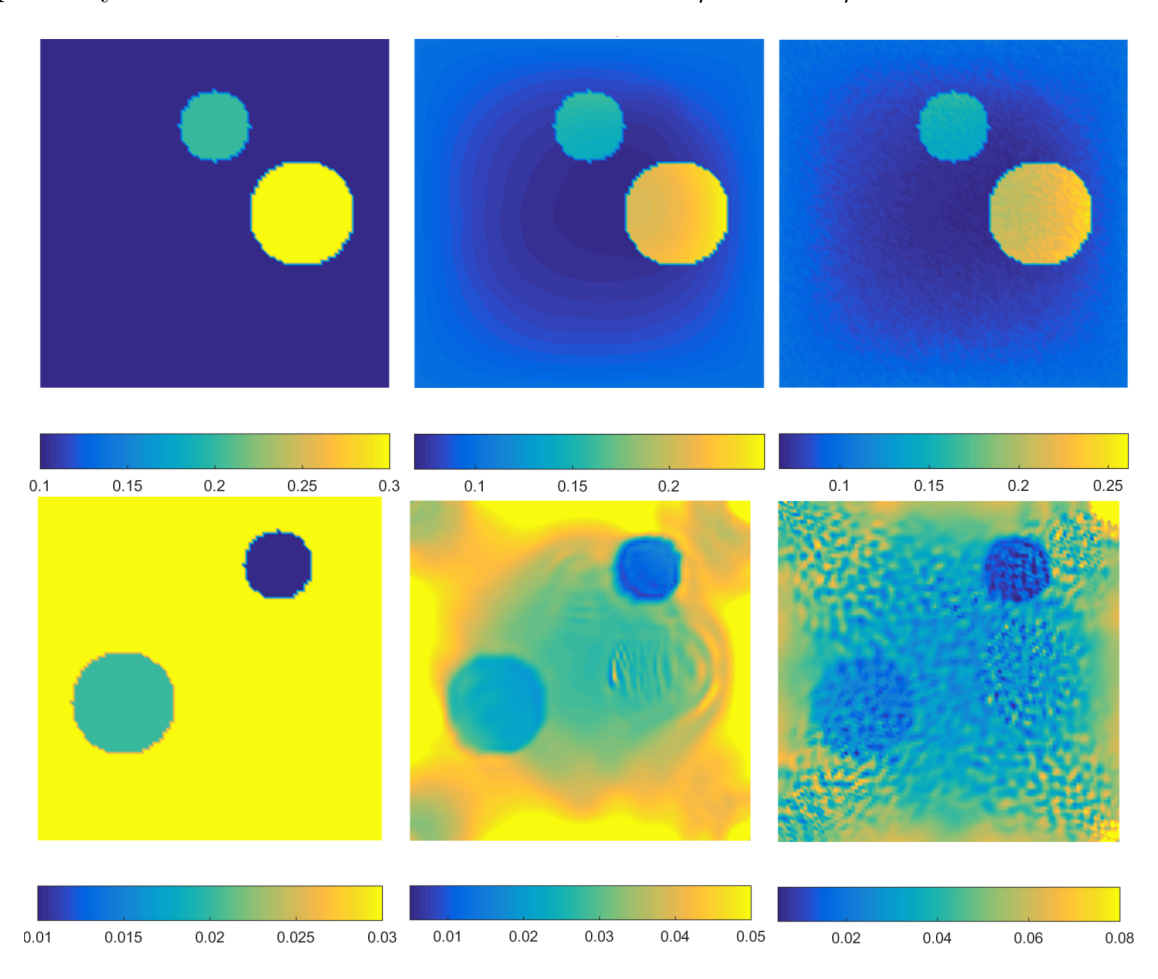


Figure 4: Reconstructions of the absorption coefficient  $\sigma_a$  (defined in (77), top row) and the diffusion coefficient (=  $1/[3(1-g)\sigma_s]$  with  $\sigma_s$  defined in (79), bottom row). Show are the true coefficients (left) and the reconstructions using noise-free data (middle) and noisy data with  $\eta = 5$  (right).

Experiment 2 [Reconstructing  $(\sigma_a, \sigma_s)$  from Acoustic Data]. In this numerical experiment, we perform simultaneous reconstruction of the absorption and the scattering coefficients. The absorption coefficient is the same as the one defined in (77) while the scattering

coefficient is defined as

$$\sigma_s(\mathbf{x}) = 85 + 260\chi_{B_2}(\mathbf{x}) + 260\chi_{B_3}(\mathbf{x}),\tag{79}$$

with  $B_3 = \{(x,y) : (x-0.5)^2 + (y-0.8)^2 \le (0.3)^2\}$  and  $B_4 = \{(x,y) : (x-1.4)^2 + (y-1.6)^2 \le (0.2)^2\}$ . We again collect data from four different illumination patterns. The reconstruction are initialized at  $\sigma_a^0 = 0.1$  and  $\sigma_s^0 = 120$ . The linear bound constraints are set as  $10 \le \sigma_s \le 500$  and  $0 \le \sigma_a \le 1$  in all cases. The regularization strength are selected at  $\alpha = 1e - 6$  and  $\beta = 1e - 10$  after a couple of trial and error testings. Note that the discrepancy between the parameter  $\alpha$  and  $\beta$  mainly come from the fact that the coefficients  $\sigma_a$  and  $\sigma_s$  have values that are different on a few orders of magnitude:  $\sigma_a \sim 0.1$  while  $\sigma_s \sim 100$ .

Noise Level	$\mathcal{E}_a = \frac{\left\ \hat{\sigma}_a - \sigma_a\right\ _{L^2}}{\left\ \sigma_a\right\ _{L^2}}$	$\mathcal{E}_s = rac{\left\ \hat{\sigma}_s - \sigma_s ight\ _{L^2}}{\left\ \sigma_s ight\ _{L^2}}$
$\eta = 0$	0.023	0.182
$\eta = 2$	0.043	0.251
$\eta = 5$	0.091	0.284
$\eta = 10$	0.174	0.385

Table 1: Relative  $L^2$  errors in the simultaneous reconstructions of the absorption and scattering coefficients given in (77) and (79) from acoustic data with different noise levels.

In Figure 4 we show the reconstructions results from clean data and noisy data with  $\eta = 5$ . The relative  $L^2$  errors in these reconstructions, as well as two additional reconstructions, are summarized in Table 1.

We observe that the quality of the reconstructions is again very high when noise level is very low. However, the quality degenerates quickly as the noise level increases, especially for the scattering coefficient. As we observed in the previous cases, the box constraints on the coefficients are very loose and do not have significant impact on the reconstructions. Tighter bounds can be imposed to improve the quality of the reconstructions when these a priori information are available. More carefully selection of the regularization coefficient might also help improve the reconstructions. Those are not the directions that we want to pursue in this research.

#### 5.2 Inversions for cross-model comparisons

The numerical tests in Experiment 1 and Experiment 2 suggest that the PAT inverse problem based on the simplified  $P_2$  model has very similar stability properties and reconstruction quality as those based on the classical diffusion model or the radiative transport model [10, 11, 51, 66], assuming that the data used in the reconstructions are generated from the same model. In the next numerical experiment, we address a different issue in PAT reconstructions. We are interested in studying the impact of model inaccuracies on the quality of the reconstructions of the absorption and the scattering coefficients. More precisely, assuming that the measurement data are generated by an accuracy model but we

perform reconstructions based on a less accurate model. We are interested in the impact of the inaccuracy of the inversion model on the reconstruction results. This problem has been studied in Theorem 4.5 for the simple case of reconstructing only the absorption coefficient. We now provide some numerical evidences.

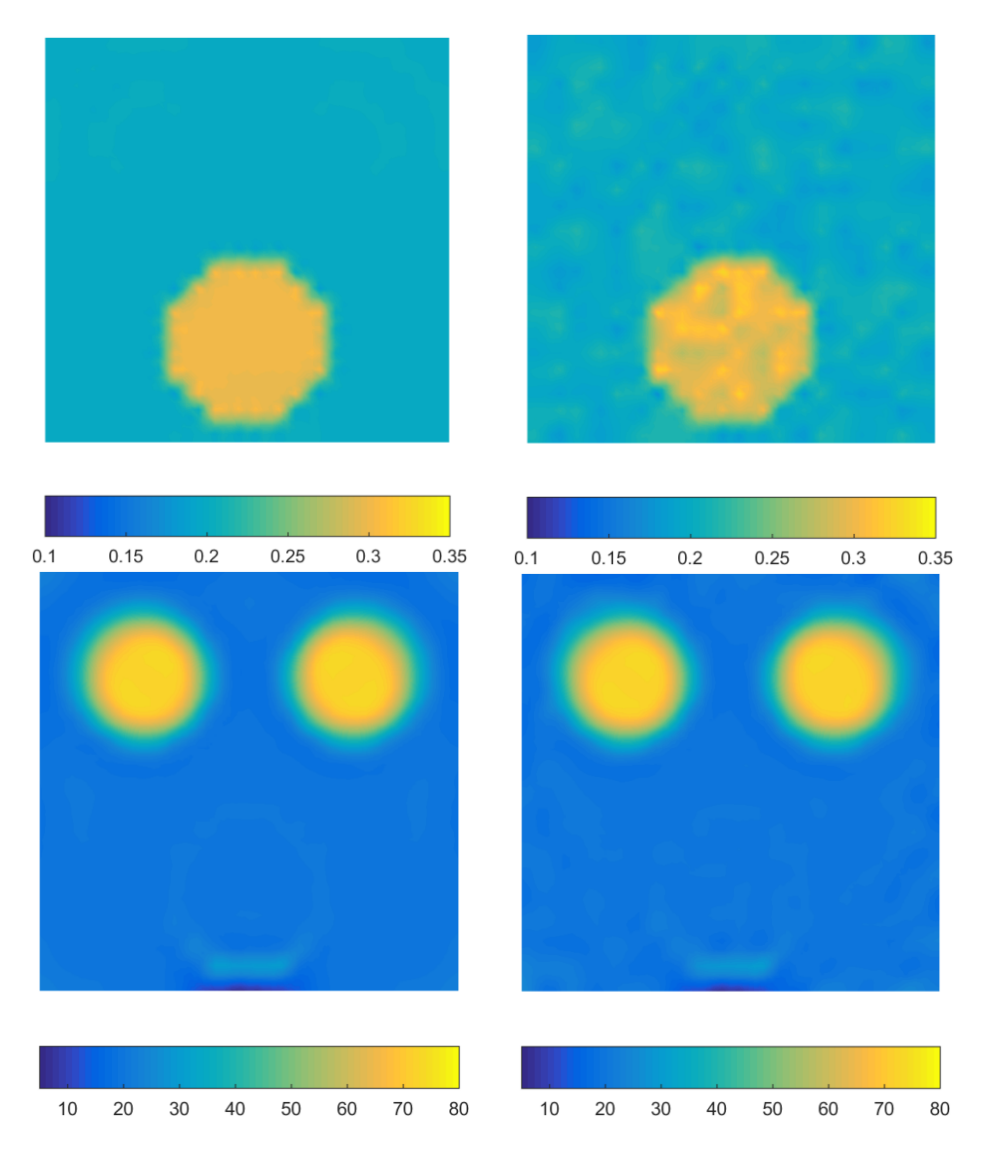


Figure 5: Reconstructions of the absorption coefficient  $\sigma_a$  (left column) and the scattering coefficient  $\sigma_s$  (right column) defined in (80) from noise-free data ( $\eta = 0$ , top row) and noisy data with  $\eta = 5$  (bottom row). The reconstructions are performed using the simplified  $P_2$  model as the forward light propagation model.

Experiment 3 [Cross-model Inversion Comparisons]. The setup is as follows. The domain is the unit square  $\Omega = (0,1) \times (0,1)$ . The true absorption and scattering coefficients are

$$\sigma_a(\mathbf{x}) = 0.2 + 0.1\chi_{B_5}(\mathbf{x}), 
\sigma_s(\mathbf{x}) = 20 + 60\chi_{B_6}(\mathbf{x}) + 60\chi_{B_7}(\mathbf{x}), \tag{80}$$

with  $B_5 = \{(x,y) : (x-0.5)^2 + (y-0.25)^2 \le (0.2)^2\}$ ,  $B_6 = \{(x,y) : (x-0.25)^2 + (y-0.75)^2 \le (0.15)^2\}$ , and  $B_7 = \{(x,y) : (x-0.75)^2 + (y-0.75)^2 \le (0.15)^2\}$ . The anisotropic factor is again g = 0.9.

We collect data from the four different illumination patterns that we used in the previous numerical experiments. The data are generated by solving the simplified  $P_2$  model with the true absorption and scattering coefficients. To exclude the impact of the acoustic wave model on the comparison, we perform reconstructions directly from the internal data H, not from the boundary ultrasound data as in the previous numerical experiments.

In all the reconstruction results below, we initialize the inversion algorithm at  $\sigma_a^0 = 0.1$  and  $\sigma_s^0 = 50$ . The linear bound constraints are set as  $10 \le \sigma_s \le 100$  and  $0 \le \sigma_a \le 1$  in all cases. The regularization strength are selected at  $\alpha = 1e - 3$  and  $\beta = 1e - 8$  after extensive numerical tests.

Noise Level	$\mathcal{E}_a = \frac{\left\ \hat{\sigma}_a - \sigma_a\right\ _{L^2}}{\left\ \sigma_a\right\ _{L^2}}$	$\mathcal{E}_s = rac{\left\ \hat{\sigma}_s - \sigma_s ight\ _{L^2}}{\left\ \sigma_s ight\ _{L^2}}$
$\eta = 0$	0.039	0.244
$\eta = 2$	0.041	0.244
$\eta = 5$	0.052	0.245
$\eta = 10$	0.079	0.250

Table 2: Relative  $L^2$  errors in the simultaneous reconstructions of the absorption and scattering coefficients in (80) based on the simplified  $P_2$  model data with different noise levels.

In Figure 5 and Figure 6 we show respectively the reconstruction results using the simplified  $P_2$  model and the classical  $P_1$  model as the model for light propagation. The relative errors in the reconstructions for the two groups of numerical simulations are summarized in Table 2 and Table 3 respectively.

A quick comparison between the first row of Figure 5 and that of Figure 6 shows that the reconstructions are significantly different, even though the internal data used in the reconstructions are the same. To be more precise, the relative  $L^2$  errors in the reconstructions changed from roughly (0.04, 0.24) in the first row of Figure 5 to roughly (0.12, 0.39) in the first row of Figure 6. This shows that the right hand side of equation (70) is relatively large, which indicates that in this specific setting, the solutions to the simplified  $P_2$  model and the classical diffusion model are quite different.

Noise Level	$\mathcal{E}_a = \frac{\ \hat{\sigma}_a - \sigma_a\ _{L^2}}{\ \sigma_a\ _{L^2}}$	$\mathcal{E}_s = rac{\left\ \hat{\sigma}_s - \sigma_s ight\ _{L^2}}{\left\ \sigma_s ight\ _{L^2}}$
$\eta = 0$	0.115	0.385
$\eta = 2$	0.116	0.388
$\eta = 5$	0.120	0.383
$\eta = 10$	0.134	0.387

Table 3: Same as Table 2 except that the reconstructions are performed using the  $P_1$  model (12) as the forward light propagation model.

The last row of Table 2 shows the reconstruction results with data containing 10% ran-

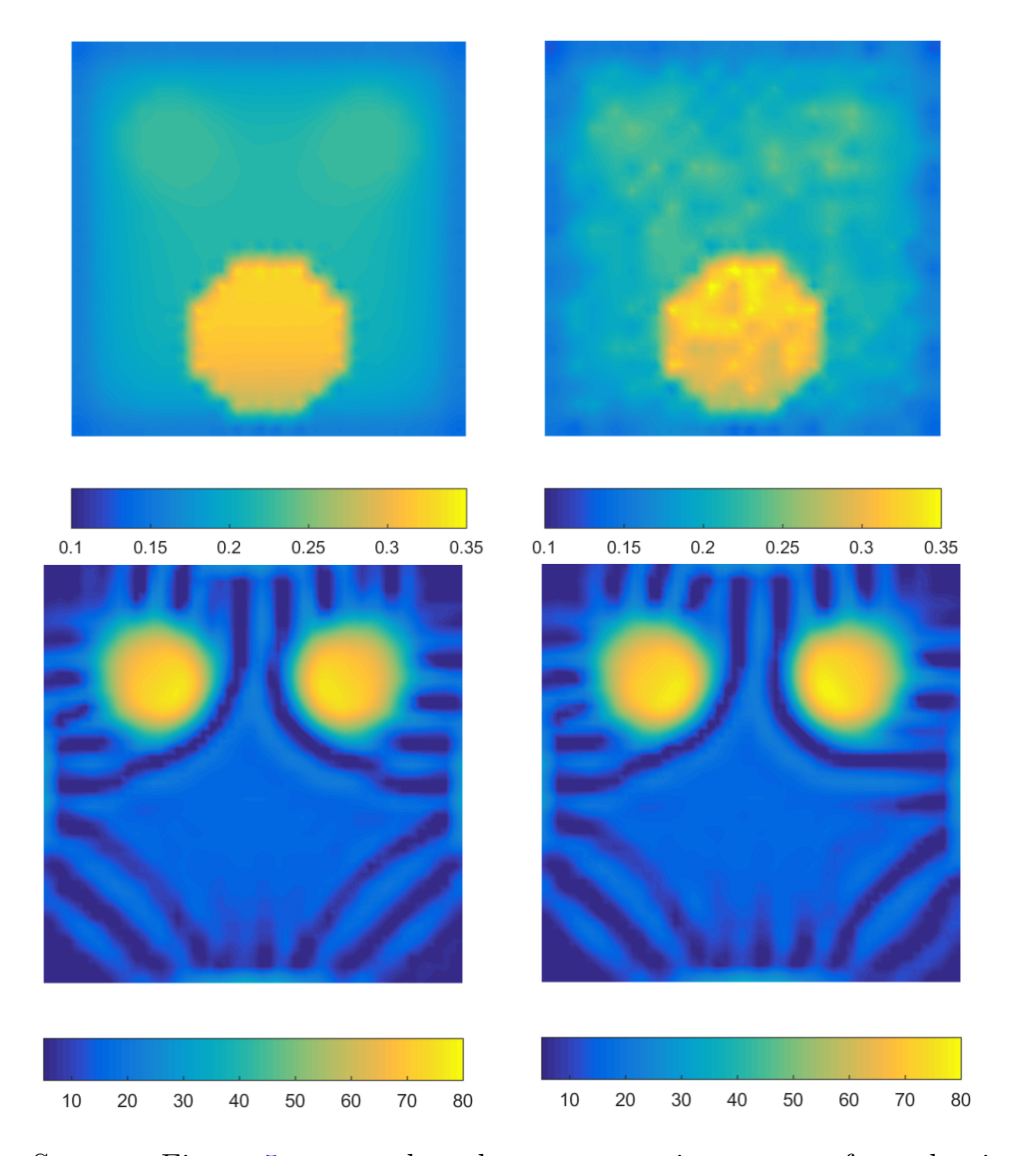


Figure 6: Same as Figure 5 except that the reconstructions are performed using the  $P_1$  model (12) as the forward light propagation model.

dom noise. Comparing the results with these in the first row of Table 3 shows that the former is still better. This implies in some sense that the "noise" we introduced here, by using the classical diffusion model (12) to replace the simplified  $P_2$  model (9), is larger than 10%. Therefore, if we believe that the data are generated with accurate model, using the same model to do PAT reconstructions gives better results than using a less accurate model. This is in general true for most of the inverse problems we know. However, for problems such as optical tomography, the benefit of using more accurate models in reconstructions is lost at relatively low noise level [16, 62, 75], which is mainly due to the severe ill-conditioning of the inversion problem. In our case, the inversion is less ill-conditioned (roughly, not mathematically speaking, although this can be characterized mathematically), and the accuracy of the forward model plays a more important role.

# 6 Concluding remarks

We studied in the paper the problem of reconstructing optical absorption and scattering coefficients in quantitative photoacoustic tomography with the simplified  $P_2$  model as the model of light propagation in the underlying medium. We showed numerically that one can reconstruct the absorption and scattering coefficients from ultrasound data generated under multiple illuminations, in a relatively stable manner. We also studied the quantitative step of the reconstructions where we developed some uniqueness and stability results under simplified circumstances.

There are multiple aspects of the current research that can be improved. One of our near future plan is to generalize method proposed in this work to the case of the multiple wavelength data. In that setup, we hope to be able to simultaneously reconstruct the absorption, and the scattering and the Grüneisen coefficients as proved in the classical diffusion case [10]. Another practically important issue to address is to perform similar reconstructions from experimentally measured ultrasound data. It would be interesting to see whether or not we can observe any difference between the reconstructions with the simplified  $P_2$  model and those with the classical diffusion model with real-world experimental data.

# Acknowledgments

This work is partially supported by the National Science Foundation through grants DMS-1321018, DMS-1620473 and DMS-1720306. S.V. would like to acknowledge partial support from the Statistical and Applied Mathematical Sciences Institute (SAMSI).

#### References

- [1] M. L. Adams and E. W. Larsen, Fast iterative methods for discrete-ordinates particle transport calculations, Prog. Nucl. Energy, 40 (2002), pp. 3–150.
- [2] M. AGRANOVSKY, P. KUCHMENT, AND L. KUNYANSKY, On reconstruction formulas and algorithms for the thermoacoustic tomography, in Photoacoustic Imaging and Spectroscopy, L. V. Wang, ed., CRC Press, 2009, pp. 89–101.
- [3] G. Ambartsoumian, R. Gouia-Zarrad, and M. Lewis, *Inversion of the circular Radon transform on an annulus*, Inverse Problems, 26 (2010). 105015.
- [4] H. Ammari, E. Bretin, J. Garnier, and A. Wahab, *Time reversal in attenuating acoustic media*, Contemporary Mathematics, 548 (2011), pp. 151–163.
- [5] H. Ammari, E. Bretin, V. Jugnon, and A. Wahab, *Photo-acoustic imaging for attenuating acoustic media*, in Mathematical Modeling in Biomedical Imaging II, H. Ammari, ed., vol. 2035 of Lecture Notes in Mathematics, Springer-Verlag, 2012, pp. 53–80.

- [6] S. R. Arridge, Optical tomography in medical imaging, Inverse Probl., 15 (1999), pp. R41– R93.
- [7] G. Bal, Inverse transport theory and applications, Inverse Problems, 25 (2009). 053001.
- [8] —, Hybrid inverse problems and internal functionals, in Inside Out: Inverse Problems and Applications, G. Uhlmann, ed., vol. 60 of Mathematical Sciences Research Institute Publications, Cambridge University Press, 2012, pp. 325–368.
- [9] G. Bal, A. Jollivet, and V. Jugnon, *Inverse transport theory of photoacoustics*, Inverse Problems, 26 (2010), 025011.
- [10] G. Bal and K. Ren, Multi-source quantitative PAT in diffusive regime, Inverse Problems, 27 (2011). 075003.
- [11] —, On multi-spectral quantitative photoacoustic tomography in diffusive regime, Inverse Problems, 28 (2012). 025010.
- [12] G. Bal and G. Uhlmann, *Inverse diffusion theory of photoacoustics*, Inverse Problems, 26 (2010). 085010.
- [13] B. Banerjee, S. Bagchi, R. M. Vasu, and D. Roy, Quatitative photoacoustic tomography from boundary pressure measurements: noniterative recovery of optical absorption coefficient from the reconstructed absorbed energy map, J. Opt. Soc. Am. A, 25 (2008), pp. 2347–2356.
- [14] P. Beard, Biomedical photoacoustic imaging, Interface Focus, 1 (2011), pp. 602–631.
- [15] P. Burgholzer, G. J. Matt, M. Haltmeier, and G. Paltauf, Exact and approximative imaging methods for photoacoustic tomography using an arbitrary detection surface, Phys. Rev. E, 75 (2007). 046706.
- [16] M. CHU AND H. DEHGHANI, Image reconstruction in diffuse optical tomography based on simplified spherical harmonics approximation, Optics Express, 17 (2009), pp. 24208–24223.
- [17] B. T. Cox, S. R. Arridge, and P. C. Beard, *Photoacoustic tomography with a limited-aperture planar sensor and a reverberant cavity*, Inverse Problems, 23 (2007), pp. S95–S112.
- [18] —, Estimating chromophore distributions from multiwavelength photoacoustic images, J. Opt. Soc. Am. A, 26 (2009), pp. 443–455.
- [19] B. T. Cox, S. R. Arridge, K. P. Köstli, and P. C. Beard, Two-dimensional quantitative photoacoustic image reconstruction of absorption distributions in scattering media by use of a simple iterative method, Applied Optics, 45 (2006), pp. 1866–1875.
- [20] B. T. COX AND P. C. BEARD, Photoacoustic tomography with a single detector in a reverberant cavity, J. Opt. Soc. Am. A, 125 (2009), pp. 1426–1436.
- [21] B. T. Cox, J. G. Laufer, and P. C. Beard, The challenges for quantitative photoacoustic imaging, Proc. of SPIE, 7177 (2009). 717713.
- [22] B. T. Cox, T. Tarvainen, and S. R. Arridge, Multiple illumination quantitative photoacoustic tomography using transport and diffusion models, in Tomography and Inverse Transport Theory, G. Bal, D. Finch, P. Kuchment, J. Schotland, P. Stefanov, and G. Uhlmann, eds., vol. 559 of Contemporary Mathematics, Amer. Math. Soc., Providence, RI, 2011, pp. 1–12.

- [23] R. Dautray and J.-L. Lions, Mathematical Analysis and Numerical Methods for Science and Technology, Vol VI, Springer-Verlag, Berlin, 1993.
- [24] T. DIERKES, O. DORN, F. NATTERER, V. PALAMODOV, AND H. SIESCHOTT, Fréchet derivatives for some bilinear inverse problems, SIAM J. Appl. Math., 62 (2002), pp. 2092–2113.
- [25] T. Ding, K. Ren, and S. Vallelian, A one-step reconstruction algorithm for quantitative photoacoustic imaging, Inverse Problems, 31 (2015), p. 095005.
- [26] R. J. DIPERNA AND P.-L. LIONS, On the Cauchy problem for Boltzmann equations: global existence and weak stability, Ann. Math., 130 (1989), pp. 321–366.
- [27] J. J. Duderstadt and W. R. Martin, *Transport Theory*, John-Wiley & Sons, Inc., New York, 1979.
- [28] L. C. Evans, *Partial Differential Equations*, American Mathematical Society, Providence, RI, 2010.
- [29] D. FINCH, M. HALTMEIER, AND RAKESH, Inversion of spherical means and the wave equation in even dimensions, SIAM J. Appl. Math., 68 (2007), pp. 392–412.
- [30] D. FINCH AND RAKESH, The spherical mean operator with centers on a sphere, Inverse Problems, 35 (2007), pp. S37–S50.
- [31] M. Frank, A. Klar, E. W. Larsen, and S. Yasuda, Time-dependent simplified  $P_N$  approximation to the equations of radiative transfer, J. Comput. Phys., 226 (2007), pp. 2289–2305.
- [32] D. GILBARG AND N. S. TRUDINGER, Elliptic Partial Differential Equations of Second Order, Springer-Verlag, Berlin, 2000.
- [33] P. E. GILL, W. MURRAY, AND M. A. SAUNDERS, SNOPT: An SQP algorithm for large-scale constrained optimization, SIAM Rev., 47 (2005), pp. 99–131.
- [34] Z. Guo, S. Wan, K. Kim, and C. Kosaraju, Comparing Diffusion Approximation with Radiation Transfer Analysis for Light Transport in Tissues, Opt. Rev., 10 (2003), pp. 415–421.
- [35] M. Haltmeier, Inversion formulas for a cylindrical Radon transform, SIAM J. Imag. Sci., 4 (2011), pp. 789–806.
- [36] M. Haltmeier, O. Scherzer, P. Burgholzer, and G. Paltauf, *Thermoacoustic computed tomography with large planer receivers*, Inverse Problems, 20 (2004), pp. 1663–1673.
- [37] M. HALTMEIER, T. SCHUSTER, AND O. SCHERZER, Filtered backprojection for thermoacoustic computed tomography in spherical geometry, Math. Methods Appl. Sci., 28 (2005), pp. 1919–1937.
- [38] Y. Hristova, Time reversal in thermoacoustic tomography an error estimate, Inverse Problems, 25 (2009). 055008.
- [39] Y. HRISTOVA, P. KUCHMENT, AND L. NGUYEN, Reconstruction and time reversal in thermoacoustic tomography in acoustically homogeneous and inhomogeneous media, Inverse Problems, 24 (2008). 055006.

- [40] V. ISAKOV, *Inverse Problems for Partial Differential Equations*, Springer-Verlag, New York, second ed., 2002.
- [41] S. L. Jacques, Optical properties of biological tissues: a review., Physics in Medicine and Biology, 58 (2013), pp. R37–R61.
- [42] A. D. Klose and E. W. Larsen, Light transport in biological tissue based on the simplified spherical harmonics equations, J. Comput. Phys., 220 (2006), pp. 441–470.
- [43] P. Kuchment, Mathematics of hybrid imaging. a brief review, in The Mathematical Legacy of Leon Ehrenpreis, I. Sabadini and D. Struppa, eds., Springer-Verlag, 2012.
- [44] P. Kuchment and L. Kunyansky, Mathematics of thermoacoustic tomography, Euro. J. Appl. Math., 19 (2008), pp. 191–224.
- [45] —, Mathematics of thermoacoustic and photoacoustic tomography, in Handbook of Mathematical Methods in Imaging, O. Scherzer, ed., Springer-Verlag, 2010, pp. 817–866.
- [46] L. Kunyansky, Explicit inversion formulae for the spherical mean Radon transform, Inverse Problems, 23 (2007), pp. 373–383.
- [47] O. A. LADYZHENSKAYA, The Boundary Value Problems of Mathematical Physics, Springer-Verlag, New York, 1985.
- [48] E. W. Larsen, G. Thömmes, A. Klar, M. Seaïdd, and T. Götze, Simplified PN approximations to the equations of radiative heat transfer and applications, J. Comput. Phys., 183 (2002), pp. 652–675.
- [49] J. LAUFER, B. T. COX, E. ZHANG, AND P. BEARD, Quantitative determination of chromophore concentrations from 2D photoacoustic images using a nonlinear model-based inversion scheme, Applied Optics, 49 (2010), pp. 1219–1233.
- [50] C. Li and L. Wang, *Photoacoustic tomography and sensing in biomedicine*, Phys. Med. Biol., 54 (2009), pp. R59–R97.
- [51] A. V. MAMONOV AND K. Ren, Quantitative photoacoustic imaging in radiative transport regime, Comm. Math. Sci., 12 (2014), pp. 201–234.
- [52] W. McLean, Strongly Elliptic Systems and Boundary Integral Equations, Cambridge University Press, Cambridge, 2000.
- [53] M. F. Modest, Radiative Heat Transfer, Academic Press, 3rd ed., 2013.
- [54] L. V. NGUYEN, A family of inversion formulas in thermoacoustic tomography, Inverse Probl. Imaging, 3 (2009), pp. 649–675.
- [55] G. Paltauf, R. Nuster, and P. Burgholzer, Weight factors for limited angle photoacoustic tomography, Phys. Med. Biol., 54 (2009), pp. 3303–3314.
- [56] S. K. Patch and O. Scherzer, *Photo- and thermo- acoustic imaging*, Inverse Problems, 23 (2007), pp. S1–S10.

- [57] A. Pulkkinen, B. T. Cox, S. R. Arridge, H. Goh, J. P. Kaipio, and T. Tarvainen, Direct estimation of optical parameters from photoacoustic time series in quantitative photoacoustic tomography, IEEE Trans. Med. Imag., 35 (2016), pp. 2497–2508.
- [58] J. Qian, P. Stefanov, G. Uhlmann, and H. Zhao, An efficient Neumann-series based algorithm for thermoacoustic and photoacoustic tomography with variable sound speed, SIAM J. Imaging Sci., 4 (2011), pp. 850–883.
- [59] Rakesh, A linearized inverse problem for the wave equation, Comm. in P.D.E., 13 (1988), pp. 573–601.
- [60] K. Ren, Recent developments in numerical techniques for transport-based medical imaging methods, Commun. Comput. Phys., 8 (2010), pp. 1–50.
- [61] K. Ren, G. Bal, and A. H. Hielscher, Frequency domain optical tomography based on the equation of radiative transfer, SIAM J. Sci. Comput., 28 (2006), pp. 1463–1489.
- [62] —, Transport- and diffusion-based optical tomography in small domains: A comparative study, Applied Optics, 46 (2007), pp. 6669–6679.
- [63] K. Ren and F. Triki, A global stability estimate for the photoacoustic inverse problem in layered media, arXiv:1707.07260, (2017).
- [64] K. Ren, R. Zhang, and Y. Zhong, Inverse transport problems in quantitative PAT for molecular imaging, Inverse Problems, 31 (2015). 125012.
- [65] J. RIPOLL AND V. NTZIACHRISTOS, Quantitative point source photoacoustic inversion formulas for scattering and absorbing media, Phys. Rev. E, 71 (2005). 031912.
- [66] T. SARATOON, T. TARVAINEN, B. T. COX, AND S. R. ARRIDGE, A gradient-based method for quantitative photoacoustic tomography using the radiative transfer equation, Inverse Problems, 29 (2013). 075006.
- [67] O. Scherzer, Handbook of Mathematical Methods in Imaging, Springer-Verlag, 2010.
- [68] P. Stefanov and G. Uhlmann, Thermoacoustic tomography with variable sound speed, Inverse Problems, 25 (2009). 075011.
- [69] C. TAO AND X. LIU, Reconstruction of high quality photoacoustic tomography with a limited-view scanning, Optics Express, 18 (2010), pp. 2760–2766.
- [70] T. Tarvainen, B. T. Cox, J. P. Kaipio, and S. R. Arridge, Reconstructing absorption and scattering distributions in quantitative photoacoustic tomography, Inv. Probl., 28 (2012). 084009.
- [71] T. Tarvainen, M. Vauhkonen, V. Kolehmainen, S. R. Arridge, and J. P. Kaipio, Coupled radiative transfer equation and diffusion approximation model for photon migration in turbid medium with low-scattering and non-scattering regions, Phys. Med. Biol., 50 (2005), pp. 4913–4930.
- [72] B. E. Treeby, E. Z. Zhang, and B. T. Cox, *Photoacoustic tomography in absorbing acoustic media using time reversal*, Inverse Problems, 26 (2010). 115003.

- [73] L. V. Wang, Ultrasound-mediated biophotonic imaging: a review of acousto-optical tomography and photo-acoustic tomography, Disease Markers, 19 (2004), pp. 123–138.
- [74] —, Tutorial on photoacoustic microscopy and computed tomography, IEEE J. Sel. Topics Quantum Electron., 14 (2008), pp. 171–179.
- [75] S. WRIGHT, M. SCHWEIGER, AND S. R. ARRIDGE, Reconstruction in optical tomography using the PN approximations, Meas. Sci. Technol., 18 (2007), pp. 79–86.
- [76] Y. Xu, L. V. Wang, G. Ambartsoumian, and P. Kuchment, Reconstructions in limited view thermoacoustic tomography, Med. Phys., 31 (2004). 724-733.
- [77] Z. Yuan, Q. Wang, and H. Jiang, Reconstruction of optical absorption coefficient maps of heterogeneous media by photoacoustic tomography coupled with diffusion equation based regularized Newton method, Optics Express, 15 (2007), pp. 18076–18081.
- [78] R. J. Zemp, Quantitative photoacoustic tomography with multiple optical sources, Applied Optics, 49 (2010), pp. 3566–3572.